ELSEVIER

Coordination Chemistry Reviews
219–221 (2001) 187–234

COORDINATION CHEMISTRY REVIEWS

www.elsevier.com/locate/ccr

Monomeric and extended oxo-centered triruthenium clusters

Henrique E. Toma *, Koiti Araki, Anamaria D.P. Alexiou, Sofia Nikolaou, Sergio Dovidauskas

Instituto de Química, Universidade de São Paulo, C. Postal 26077 CEP 05513-970, São Paulo, SP, Brazil

Received 20 September 2000; accepted 19 December 2000

Dedicated to Professor Alfred B. Lever on the occasion of his 65th birthday

Contents

* Corresponding author. Tel.: +55-11-3818-3887; fax: +55-11-3815-5579.
E-mail address: henetoma@iq.usp.br (H.E. Toma).

PII: S0010-8545(01)00326-5

Abstract

The chemistry of μ-oxo-centered trinuclear ruthenium-carboxylate clusters, of general formula $[Ru_3O(RCO_2)_6L_3]^n$, has been dealt with special emphasis on their spectroscopic and electrochemical properties, as well as their capability to form ligand-bridged oligomeric structures exhibiting pronounced electronic delocalization. Mixed systems containing trinuclear ruthenium clusters attached to transition metal complexes and porphyrins are also focused upon in this review article, from the point of view of cooperative interactions and supramolecular chemistry. The role of the trinuclear clusters as electron donor/acceptor groups, and their relevance in biomimetic systems, redox catalysis and molecular devices have been discussed.

Keywords: Oxo-ruthenium clusters; Ruthenium acetate clusters; Metal clusters; Trinuclear ruthenium clusters

1. Introduction

Trinuclear μ-oxo-centered ruthenium-carboxylate clusters, of general formula $[Ru_3O(RCO_2)_6L_3]^n$, where R = H [1], CH_3 [2–4], C_2H_5 [2,5], C_3H_7 [2], C_3F_7 [6], C_6H_5 [2,7,8], C_7H_{15} [2], C_8H_{16} [2], and L = H_2O, PPh_3, CO, *N*-heterocycles, $OS(CH_3)_2$, etc. have been extensively investigated in the last decade, because of their rich mixed-valence chemistry, and catalytic properties. This type of complex exhibits a triangular structure strongly held by a central μ-oxo-bridge, as well as by three double carboxylate bridges (Fig. 1). The close proximity of the metal ions gives rise to strong electronic and magnetic interactions, stabilizing a whole series of successive oxidation states, associated with each Ru^{II}, Ru^{III} or Ru^{IV} center.

Several review articles dealing with general aspects of ruthenium clusters [9–14] have been published since 1968; however, the great development of the supramolecular chemistry of the $[Ru_3O(RCO_2)_6L_3]^n$ complexes in the last decade, particularly in the field of extended interactions, justify a more comprehensive report on this subject.

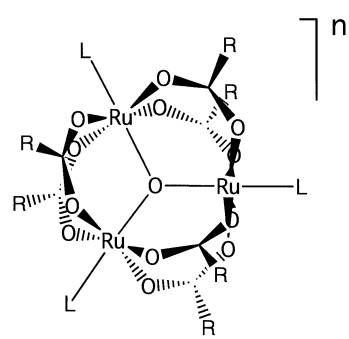

Fig. 1. Schematic representation of the oxo-centered trinuclear ruthenium clusters structure. R = carboxylate ligands and L = H_2O, MeOH or *N*-heterocyclic ligands.

2. Monomeric trinuclear clusters

2.1. Synthetic aspects

The basic procedure employed in the synthesis of substituted trinuclear ruthenium clusters has been described by Spencer and Wilkinson [2]. It is based on the formation of the precursor complex $[Ru_3O(RCO_2)_6S_3]^+$ ($S = H_2O$, MeOH or EtOH), by refluxing ethanol solutions containing $RuCl_3 \cdot nH_2O$, RCO_2H, $NaRCO_2$, as shown in Scheme 1.

The precursor complexes can be isolated as green solids of composition $[Ru_3O(RCO_2)_6S_3]X$ ($X = RCO_2^-$ [2], ClO_4^- [15,16], BF_4^- [1] or PF_6^- [17]) or stored in solution for a long period of time, with no evidence of decomposition [3]. The kinetics and mechanism of the reaction involved have not been investigated; however, the participation of the intermediate binuclear complex $Ru_2O(Ac)_2$, has been suggested [18,19] which would explain the formation of mixed clusters of the type Ru_2M, but not RuM_2 (Ac, acetate).

Substitution of the solvent molecules in the precursor complex proceeds rapidly in the presence of coordinating ligands, L, allowing the preparation of a large number of symmetrically substituted clusters $[Ru_3O(RCO_2)_6L_3]^+$ [2–4,16,17,20–25]. Another contrasting route for the preparation of this type of cluster has been described by Zhilyaev et al. [5], by refluxing $[Ru_2(SO_4)_2(OH_2)_2L_4]$ in RCO_2H.

The direct synthesis of mixed ligand clusters of the type $[Ru_3O(Ac)_6L_2L']^n$, starting from the precursor complex in the presence of L and L′, has not been reported up to the present time. A possible route [20,26–28] involves the reduction of the precursor complex followed by reaction with CO, yielding $[Ru_3O(Ac)_6(CO)S_2]$, where S = solvent. This complex undergoes substitution of the solvent molecules by L, and after this, the corresponding $[Ru_3O(Ac)_6(CO)L_2]$ species can be oxidized with bromine in order to eliminate the CO ligand. By adding L′, the ligand mixed cluster $[Ru_3O(Ac)_6L_2L']^+$ can be obtained. Another procedure [3,25,29–31] starts from the substituted symmetric cluster, $[Ru_3O(Ac)_6L_3]^+$. After reducing with N_2H_4, the product can be converted into $[Ru_3O(Ac)_6L_2CO]$ by treating with CO. Then, oxidation with bromine followed by the addition of L′ yields the $[Ru_3O(Ac)_6L_2L']$ cluster.

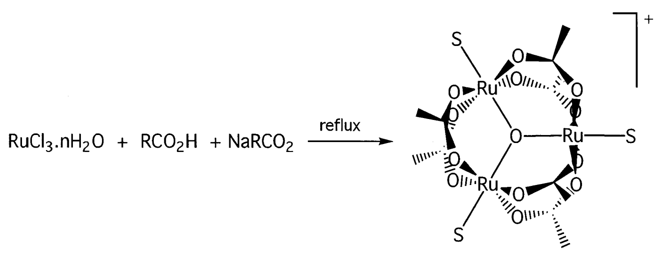

Scheme 1.

In the case of the asymmetric cluster $[Ru_3O(Ac)_6(L)(L')L'']^+$ a similar procedure has been employed, starting from $[Ru_3O(Ac)_6(CO)S_2]$. By reacting this complex with L, but using less than stoichiometric (1:1) amounts of L, the intermediate species $[Ru_3O(Ac)_6(CO)(L)S]$ can be generated. Substitution of S by L′, leads to the $[Ru_3O(Ac)_6(CO)(L)L']$ product, which can be oxidized with bromine in order to remove the CO ligand, and to allow the addition of L″, yielding $[Ru_3O(Ac)_6(L)(L')(L'')]$ [27,32,33].

2.2. Structural aspects

Relevant X-ray structural data for some $[Ru_3O(Ac)_6L_3]^{n+}$ and related clusters are collected in Table 1. Most of the complexes exhibit the three metal atoms in an equilateral triangle [34] arrangement, except the clusters containing CO or isocyanide ligands, which are better described as an isosceles triangle [28,35,36]. In all the cases, the oxygen atom is located at the center of the triangular plane. In addition, there are six carboxylate bridging groups and three axial ligands L or L′ *trans* to the central oxygen atom.

The Ru–Ru, $Ru–O_{central}$ and $Ru–O_{acetate}$ bond lengths are not sensitive to the changes in the formal oxidation states of the metal ion, implying a strong electronic delocalization within the Ru_3O^{m+} core. The Ru–L bond is significantly longer than the $Ru–O_{central}$ and $Ru–O_{acetate}$ distances, reflecting a *trans*-influence from the central oxygen atom.

In the case of the asymmetric $[Ru_3O(Ac)_6L_2(CO)]$ clusters, the formal oxidation state is $Ru_3^{III,III,II}O$ and it has been suggested that CO would stabilize preferentially the Ru^{II} site [28], leading to a partially localized valence system. A similar effect is observed for the cluster $[Ru_3O(Ac)_6(CNXy)(py)_2]\cdot 2CHCl_3$ [35,36], where CNXy, xylyl isocyanide ligand and py, pyridine.

Because of the high symmetry of the trinuclear ruthenium clusters, NMR spectroscopy provides the most powerful way to probe their structural characteristics in solution. Several ^{1}H-NMR [2,3,7,15,17,20,27,28,30,32,34–48], ^{13}C-NMR [7,15,30,40,43,49,50] and ^{19}F-NMR [6,51] spectral studies have been reported in the literature. The most representative data can be seen in Table 2.

In the case of symmetric clusters in the formal $Ru_3^{III,III,III}$ oxidation state, e.g. $[Ru_3O(Ac)_6(py)_3]^+$, the acetate protons give rise to a single peak around 5 ppm. The equivalence is removed in the case of the less symmetric clusters, $[Ru_3O(Ac)_6L_2L']^+$, as indicated by the splitting of the acetate proton signals into two peaks, exhibiting 1:2 relative intensities (see Table 2). The protons of the axial ligands (L) are also very sensitive to the symmetry changes in the clusters. It has been observed that for coordinated *N*-heterocyclic ligands such as pyridine, the protons at the *ortho* position (H_α) are strongly sensitive to the local paramagnetic effects induced by the metal centers, shifting to higher field regions (around 0 ppm) with respect to the *meta* (H_β) and *para* (H_γ) protons.

For the less symmetric clusters, e.g. $[Ru_3O(Ac)_6L_2L']^+$, the ^{1}H-NMR signals for the L′ ligands and the opposing acetate (denoted here as *trans*-acetate) are mutually correlated, reflecting the existence of a *trans*-influence in the system. In addition, a

linear correlation has been observed for the *trans*-acetate signals and the pK_a of the corresponding L′ ligands [30].

As one can see in Table 2, the ^{1}H-NMR chemical shifts are very sensitive to the oxidation states of the trinuclear clusters. The acetate signals shift from 5 to 2 ppm, as the oxidation state is reduced by one, to the $Ru_3O^{III,III,II}$ complex. The reduction seems to be accompanied by a significant change in the paramagnetic anisotropy of

Table 1
Selected bond lengths (Å) for $[M_3O(RCOO)_6L_3]X$ and $[\{Ru_3O(Ac)_6(abco)(CO)\}_2(\mu\text{-pz})] \cdot 2CH_2Cl_2$ complexes

Compound	$Ru–O_{central}$	Ru–Ru	Ru–L	$Ru–O_{acetate}$ [a]
III, III, II				
$[Ru_3O(H_3CCOO)_6(PPh_3)_3]$ [34]	1.95 (2)	3.316 (3)	2.425 (7)	
	1.94 (1)	3.329 (3)	2.416 (7)	2.06(2)
	1.87 (2)	3.342 (3)	2.400 (8)	
$[Ru_2NiO(H_3CCOO)_6(py)_3] \cdot py$ [61]	1.9318(7)	3.346 (1)	2.136(6)	2.054(4)
$[Ru_2CoO(H_3CCOO)_6(py)_3] \cdot py$ [61]	1.9394 (8)	3.359 (1)	2.174 (5)	2.061(3)
$[Ru_3O(H_3CCOO)_6(CNXy)(py)_2] \cdot 2HCCl_3$ [35]	2.035 (3)	3.3909 (4)	1.880 (5)	2.073(3)
	1.888 (1)	3.2840 (7)	2.139 (3)	2.043(3)
$[Ru_3O(H_3CCOO)_6(mbpy^+)_2(CO)](ClO_4)_2 \cdot 2DMF$ [28]	2.039 (11)	3.410 (2)	1.839 (20)	2.044(5)
	1.894 (6)	3.276 (2)	2.126 (10)	
	2.065(3)	3.4217(5)	1.851(6)	
$[Ru_3O(H_3CCOO)_6(abco)_2(CO)](ClO_4)_2 \cdot CH_2Cl_2$ [36]	1.894(3)	3.4084(6)	2.261(4)	2.04(1)
	1.888(3)	3.2979(5)	2.272(4)	
$[\{Ru_3O(CH_3CO_2)_6(abco)(CO)\}_2(\mu\text{-pz})] \cdot 2CH_2Cl_2$ [36]	2.057(4)	3.4340(5)	1.838(8)	
	1.889(5)	3.3973(9)	2.115(7)	2.04(2)
	1.896(3)	3.2892(8)	2.252(4)	
III, III, III				
$[Ru_3O(H_3CCOO)_6(H_2O)_3]BF_4 \cdot 3H_2O$ [1]	1.93(2)	3.33 (1)	2.09 (2)	2.035(2)
	1.890 (1)	3.322 (2)	2.120 (1)	
$[Ru_3O(H_3CCOO)_6(H_2O)_3]BF_4 \cdot 2H_2O$ [1]	1.910 (1)	3.294 (2)	2.130 (1)	2.03(1)
	1.916 (9)	3.288 (2)	2.140 (1)	
	1.906 (6)	3.305 (1)	2.121 (7)	
$[Ru_3O(H_3CCOO)_6(H_2O)_3]ClO_4 \cdot 2H_2O$ [132]	1.912 (7)	3.296 (1)	2.107 (8)	1.999(2)
	1.904 (6)	3.310 (1)	2.089 (8)	
$[Ru_3O(H_5C_2COO)_6(py)_3]PF_6$ [5]	1.921 (8)	3.340 (3)	2.10 (2)	2.022(4)
	1.94 (2)		2.13 (2)	
$[Ru_3O(H_5C_6COO)_6(py)_3]PF_6$ [7]	1.935 (2)	3.350 (2)	2.134 (8)	2.019(6)
IV, III, III				
	1.939 (25)	3.299 (5)	2.130 (21)	
$[Ru_3O(H_3CCOO)_6(H_2O)_3](ClO_4)_2 \cdot H_2O$ [1]	1.976 (25)	3.299 (6)	2.134 (20)	2.02
	1.801 (40)	3.295 (6)	2.008 (43)	

[a] Average values.

Table 2
^{1}H-NMR data (δ, ppm) for ruthenium acetate clusters. Superscript letters denote: (a) CD_3CN; (b) CD_2Cl_2; (c) D_2O

Compound	$\delta(CH_3)$	$\delta(H_\alpha py)$	$\delta(H_\beta py)$	$\delta(H_\gamma py)$	References
III, III, III					
$[Ru_3Oac_6(py)_3]PF_6^a$ (**1**)	4.82	0.25	5.82	6.57	[30]
$[Ru_3Oac_6(py)_2(pz)]PF_6^a$ (**2**)	5.48	0.20	5.67	6.68	[39]
	5.14				
$[Ru_3Oac_6(py)_2(acpy)]PF_6^a$ (**3**)	5.07	0.28	5.77	6.60	[30]
	4.92				
$[Ru_3Oac_6(py)_2(bipy)]PF_6^a$ (**4**)	5.00	0.13	5.75	6.57	[30]
	4.89				
$[Ru_3Oac_6(py)_2(vpy)]PF_6^a$ (**5**)	4.83	0.17	5.81	6.50	[30]
	4.79				
$[Ru_3Oac_6(mbpy)_2(py)](ClO_4)_3^a$ (**6**)	5.04	0.15	5.65	6.61	[28]
	5.29				
$[Ru_2RhOAc_6(py)_3]ClO_4^b$ (**7**)	1.96	8.91	7.74	8.14	[15]
	2.42	8.60	7.96	8.11	
$[Ru_2CoOAc_6(py)_3]I_3^b$ (**8**)	0.10	9.79	17.6	3.80	[37]
	12.55	6.30	7.88	7.30	
III, III, II					
$[Ru_3Oac_6(py)_3]^b$ (**9**)	2.14	9.02	7.69	7.99	[3]
$[Ru_3Oac_6(CO)(py)_2]^a$ (**10**)	2.10	9.14	8.13	8.31	[40]
	2.16				
$[Ru_3Oac_6(py)_2(pz)]^b$ (**11**)	2.04	9.30	7.79	8.03	[3]
	2.09				
$[Ru_3Oac_6(py)(H_2O)(CO)]^c$ (**12**)	1.99	9.62	8.27	8.61	[32]
	1.97				
	1.76				
$[Ru_2CoOAc_6(py)_3]^b$ (**13**)	−5.42	12.65	10.40	9.01	[37]
	29.27				

the metal ions, shifting the position of the H_α, H_β and H_γ peaks to down field regions (around 9 ppm).

The assignment of the ^{13}C-NMR spectra of $[Ru_3O(Ac)_6L_3]^+$ clusters has been carried out on a tentative basis. Recently, however, it has been shown using two-dimensional NMR methods, such as HETCOR and HMBC [50] that the previous ^{13}C-NMR work should be revised. Such methods are required, since they provide multiple correlation between the several signals, minimizing the possibility of errors in the spectral assignment. Based on two-dimensional methods, the ^{13}C signals for the coordinated acetate ligands have been ascribed to peaks observed around −6 (CH_3) and 197 ppm (C=O), while those for the *N*-heterocyclic ligands have been located in the range of 110–150 ppm. The ^{13}C chemical shifts for the methyl (acetate) groups vary from −7.0 to −2.3 ppm as the pK_a of L increases from 3.60 to 9.39, reflecting a pronounced influence of the ligand L basicity on the acetate groups, through the triangular metal cluster.

Vibrational spectroscopy has also been extensively employed in the characterization of the trinuclear clusters. The assignment of the vibrational spectra of the $[Ru_3O(RCO_2)_6]^{0/+}$ core has been discussed [16,52] and in general the vibrations of the carboxylate ligands are not dramatically sensitive to perturbations on the trinuclear center, allowing comparisons with related complexes and ligands. In the cases of mixed clusters of the type $[Ru_2MO(Ac)_6L_3]^n$ ($n=0$, M = Mn [8], Co [8,37,53], Ni [8], Zn [8]; $n=1$, M = Rh [8,15], Co [37], L = H_2O and py), the carboxylate antisymmetric stretching vibration, ν_{as}(COO) can give rise to two bands, reflecting their C_{2v} symmetry. In the formal mixed-valence $Ru_3^{III,III,II}$ state, there is no evidence of splitting of the vibrational peaks, consistent with the pronounced electronic delocalization in this system. Perhaps, an exception is the $[Ru_3O(Ac)_6(py)_2CO]$ complex, where the presence of the strongly acceptor CO ligand seems to trap the Ru^{II} valence state, leading to a splitting of ν_{as}(COO) [3]. For this system, the vibrational spectra have been recorded at several applied potentials [54]. The carbonyl stretching frequency increases with the oxidation of the central cluster core; however, the effect is specially pronounced for the oxidation of the formal Ru^{II} site bound to CO.

An unusual redox state dependent band shape effect has been recently observed [46] in the infrared spectra of trinuclear ruthenium clusters containing terminal isocyanide ligands, i.e. $[Ru_3O(Ac)_6(CN\text{-}R)_3]$, where R = xylyl and *tert*-butyl groups. While the $Ru_3^{III,III,III}O$ and $Ru_3^{IV,III,III}O$ states exhibit a single ν(CN) sharp peak at 2168 and 2200 cm^{-1}, the $Ru_3^{III,III,II}O$ and $Ru_3^{III,II,II}O$ states exhibit a rather broad signal centered at 2094 and 1954 cm^{-1}, accompanied by a shoulder at 1990 and 2020 cm^{-1}, respectively. The structured broad bands in the last two cases have been ascribed to Fermi resonances involving the ν(CN) mode, modified by the coordination effect, and an overtone of another ligand-based mode with the appropriate energy.

Photoelectron spectroscopy and related techniques have also been employed in the characterization of the trinuclear ruthenium complexes [3,15,49,53,55,56]. Magnetic susceptibility measurements [2,20,57–59] have indicated that the $Ru_3^{III,III,II}O$ clusters are diamagnetic, while the $Ru_3^{III,III,III}O$ ones are paramagnetic. Such studies have been extended to the mixed clusters $[Ru_2MO(Ac)_6L_3]^n$, where M^{II} = Ru [60], Mg [60,61], Mn [61,62], Co [37,53,61,62], Ni [61,62], Zn [60,61] and M^{III} = Cr [18,62], Fe [62], Co [37], Ru [63], Rh [60]. In general, the Ru^{III} ions exhibit strong antiferromagnetic coupling, mainly through the oxo-bridge. The magnetic interactions with the M^{II} ions are much weaker.

2.3. Kinetic behavior

Substitution reactions in the $[Ru_3O(Ac)_6L_3]^{0/+}$ clusters have been reported in the literature for a relatively small number of systems [15,40,47,64–66]. As compared with the substitution properties of the $[Ru(H_2O)_6]^{3+}$ complex, the rates for the $[Ru_3O(Ac)_6(H_2O)_3]^+$ species are about 10^3 faster, suggesting a strong *trans*-labilizing effect from the central oxygen atom [15,64–66]. A dissociative type of mechanism has been suggested for the substitution reactions in the trinuclear ruthenium

clusters [64,66]. The stepwise kinetics involved in the reaction of the $[Ru_3O(Ac)_6(H_2O)_3]^+$ species with L, to yield the corresponding $[Ru_3O(Ac)_6L_3]^+$ products has not been completely solved [64].

For typical donor ligands, the substitution rates for the clusters at the $Ru_3^{III,III,III}O$ oxidation state can be slower than for the $Ru_3^{III,III,II}O$ case, however, the situation is inverted for complexes such as $[Ru_3O(Ac)_6(py)_2CO]$ where the presence of the CO ligand has a dramatic effect on the stabilization of the lower oxidation state. The substitution rates for the axial ligands L are also sensitive to the nature of the carboxylate ligands. For instance, the $[Ru_3O(C_6H_5CO_2)_6(py)_3]^+$ cluster derived from benzoic acid, undergoes substitution of the pyridine ligands ten times slower than for the corresponding acetate species [7].

An interesting result has been reported for asymmetric clusters of the type $[Ru_2MO(Ac)_6(py)_3]$ where $M = Zn^{II}$ and Mg^{II} ions [47]. The intrinsic lability of the Zn^{II} and Mg^{II} ions is reflected in the rapid substitution of the pyridine ligands coordinated at these sites (e.g. $10^2\ s^{-1}$, at $-50°C$, in CD_2Cl_2), as compared with the substitution rates around $10^{-4}\ s^{-1}$ for the Ru^{III} sites. The labilization effect induced by the Zn^{II} and Mg^{II} ions on the ruthenium sites is evidenced by the rather slow substitution rates on the $[Ru_3O(Ac)_6(py)_3]^+$ complex ($k = 2.4 \times 10^{-7}\ s^{-1}$, in acetonitrile).

2.4. Electrochemical and spectroelectrochemical behavior

The $[Ru_3O(Ac)_6L_3]^n$ clusters are characterized by a rather rich electrochemical behavior, exhibiting a series of four or five reversible, monoelectronic redox waves in the $+2.5$ to -1.5 V (E vs. SHE) range [67], as illustrated in Fig. 2. The oxidation states involved in this potential range can be formally expressed as $Ru_3^{IV,IV,III}O/Ru_3^{IV,III,III}O/Ru_3^{III,III,III}O/Ru_3^{III,III,II}O/Ru_3^{III,II,II}O/Ru_3^{II,II,II}O$. A remarkable point is that the first four waves are separated by ~ 1 V, reflecting an extensive electronic delocalization in the molecule. The associated redox potentials are dependent on the donor–acceptor properties of the axial ligands, L, as expressed by the linear energy relationships between $E°$ and $pK_a(L)$ previously reported in the literature (Fig. 3) [4]. The dependence of the redox potentials with the $pK_a(L)$ reflects the relative affinities of the oxidized and reduced cluster species to the axial ligands. As the pK_a of the ligand increases, the higher oxidation states are stabilized, mainly via σ-bonding effects, leading to a general decrease of $E°$. On the other hand, at lower oxidation states, the ruthenium complexes are strongly stabilized by backbonding interactions with π-acceptor ligands. This effect also contributes for the decrease of $E°$ vs. pK_a plot slope, leading to a higher dependence for the lower oxidation state species. Analyzing the potentials for the various redox processes of the ruthenium cluster species and their trends, one can infer that the $Ru_3^{III,II,II}O/Ru_3^{II,II,II}O$ couple should appear below -1.6 V and exhibit even greater dependence with pK_a. Although in most cases the measurements were limited by the potential window of the solvent, the available experimental data do not follow the expected behavior for the $Ru_3^{III,II,II}O/Ru_3^{II,II,II}O$ redox couple. Instead, reduction of the axial ligands, L, also takes place at very negative potentials.

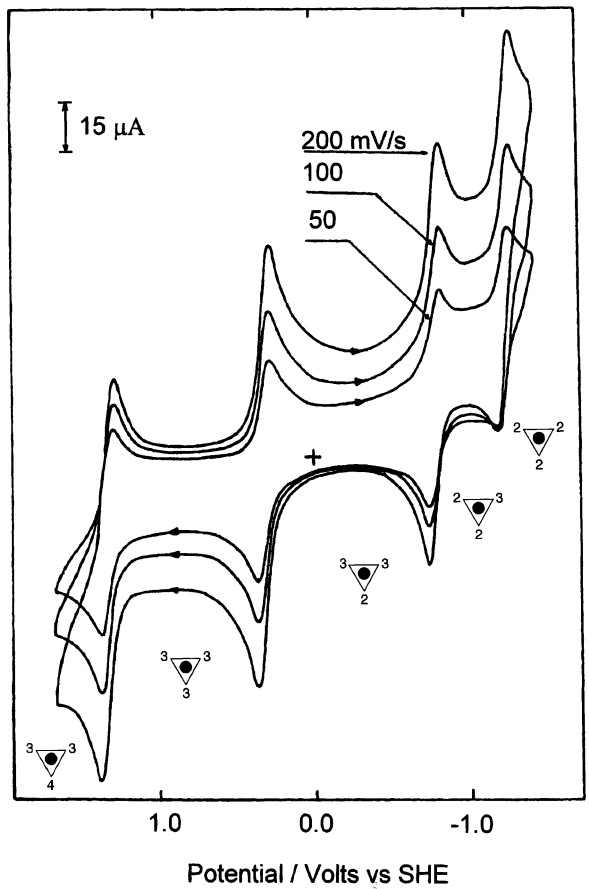

Fig. 2. Cyclic voltammograms of the $[Ru_3O(Ac)_6(pz)_3]$ cluster (3 mM) obtained at several potential scan rates, in acetonitrile ($[NEt_4ClO_4]$ 0.1 M), in the 2.0 to −2.0 V range.

The dependence of the $E°$ as a function of the ligand properties [25] has also been shown by the linear correlation with the E_L parameter proposed by Lever [68], i.e.

$$E° = S_M\left[\sum E_L\right] + I_M$$

In this equation, the S_M and I_M terms reflects the relative metal–ligand L affinities, for the two oxidation states involved. As the average oxidation state decreases, e.g. in the $Ru_3^{III,III,II}O/Ru_3^{III,II,II}O$ couple, the preference for π-acceptor ligands increases, as reflected in the equations:

$$E°(Ru_3^{IV,IV,III/IV,III,III}O) = 0.48\Sigma E_L + 1.80$$
$$E°(Ru_3^{IV,III,III/III,III,III}O) = 0.38\Sigma E_L + 0.92$$
$$E°(Ru_3^{III,III,III/III,III,II}O) = 0.76\Sigma E_L - 0.38$$
$$E°(Ru_3^{III,III,II/III,II,II}O) = 1.03\Sigma E_L - 1.83$$

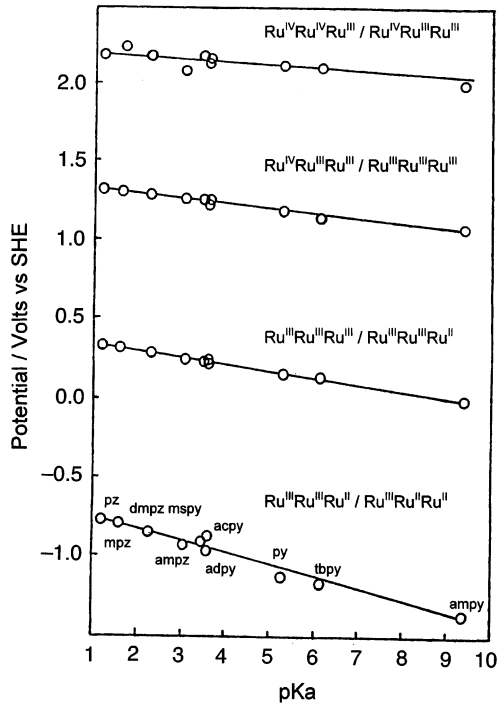

Fig. 3. Plots of the redox potentials of the $[Ru_3O(Ac)_6(L)_3]$ clusters vs. the pK_a of the *N*-heterocyclic ligands L: pz, pyrazine; py, pyridine; mpz, methylpyrazine; dmpz, 2,6-dimethylpyrazine; ampz, 2-aminopyrazine; mspy, 4-carboxymethylpyridine; acpy, 4-acetylpyridine; adpy, isonicotinamide; tbpy, 4-*tert*-butylpyridine; and ampy, 4-aminepyridine.

The I_M term involves a number of contributions, such as the ionization energy in the gas phase, electronic repulsion, solvation energy, etc. as previously discussed by Lever [68]. An interesting observation, however, is that the values of I_M vary according to the quadratic function $I_M = \alpha q + \beta q^2$, with respect to the average oxidation number q, reflecting predominantly the trends in the successive ionization potentials of the Ru_3O core. It should be noticed that this behavior is essentially identical to that observed for successive ionization energies (E) of atoms, where $dE/dq = \chi$ defines Mulliken–Jaffe electronegativity [69]. Analogously, the first derivative leads to a linear dependence of χ vs. q, where $\alpha = -4.52$ V and $\beta = 1.44$ V.

The electronic spectra of the $[Ru_3O(Ac)_6L_3]^+$ clusters consist of a broad, composite band around 700 nm, characteristic of the oxo-bridged trinuclear center, and another band in the 300–400 nm range, sensitive to the nature of L [3,4,6,7,21,22,28,31,67]. The discussion of the electronic transitions has been carried out assuming the simplified molecular orbital scheme proposed by Cotton and Norman [34], and Baumann et al. [3] for the Ru_3O center. According to this model, the central oxygen atom is considered to be sp^2 hybridized in order to account for

the Ru_3O σ-bonding framework, leaving a single p_π orbital, of a_2'' representation under D_{3h} symmetry. The ruthenium atoms can be appropriately oriented so that the d_{yz} orbitals can combine with the p_π orbitals, giving rise to a non-bonding e″ molecular orbital, and two a_2'' molecular orbitals. The lowest a_2'' level should be largely oxygen in character, while the highest a_2'' antibonding level is largely Ru in character.

Appropriate combination of the three Ru d_{xz} orbitals under D_{3h} symmetry gives rise to the e_1' and a_2' metal–metal levels, lying in the plane of the triangular cluster. The remaining Ru $d_{x^2-y^2}$ orbitals are of appropriate symmetry to interact, but only to a minor extent, since they are quite far apart. Such interaction is however enough to remove the degeneracy of the three $d_{x^2-y^2}$ orbitals, yielding the corresponding e_2' and a_1' levels.

A qualitative molecular orbital diagram, including the axial ligand π-levels, can be seen in Fig. 4.

The π-axial ligands can interact with the ruthenium d_π orbitals at the three Ru sites. If the plane of the ligand is parallel to the plane of the cluster, the interactions would involve the Ru_3O orbitals of a_2'' and e″ symmetry, while the interactions would occur with a_2' or e′ if the ligand plane is perpendicular. Consequently, rotation of the axial ligands would affect these four orbitals.

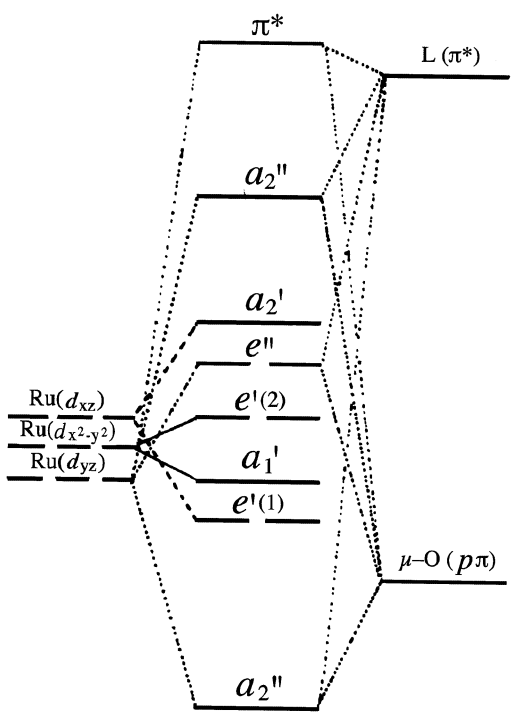

Fig. 4. Qualitative molecular orbital for the $[Ru_3O(Ac)_6(L)_3]$ in D_{3h} symmetry.

The $[Ru_3O(Ac)_6L_3]^+$ complexes, in the formal $Ru_3^{III,III,III}O$ oxidation state, have the electronic configuration $(a_2'')^2(e_1')^4(a_1')^2(e_2')^4(e'')^4(a_2')$ with an empty a_2'' orbital. For the $[Ru_3O(Ac)_6(pz)_3]^+$ complex, deconvolution of the absorption band at 710 nm leads to two main components at 715 and 630 nm and another weak one at 510 nm, ascribed to the symmetry-allowed $e'' \rightarrow a_2''$ and $a_1' \rightarrow a_2''$ transitions, and to the $e_1' \rightarrow a_2''$ electric dipole forbidden transition, respectively. From the spectroelectrochemical measurements (Fig. 5), the corresponding transitions in the $Ru_3^{IV,III,III}O$, $Ru_3^{III,III,II}O$ and $Ru_3^{III,II,II}O$ species, have been detected at 588, 540, 430; 930, 780, 615; and 1150, 957, 795 nm, respectively [67]. The optical energies follow the oxidation states, reflecting a gradual rise of the occupied d_π levels as the number of electrons increases. In the case of the totally reduced $Ru_3^{II,II,II}O$ cluster species, the d_π orbitals are completely filled and no metal–metal band is observed. In contrast, the $Ru_3^{IV,III,III}O$ cluster exhibits two vacant levels, and an additional metal–metal band at 785 nm has been ascribed to the $e_1' \rightarrow a_2'$ transition. The *N*-heterocyclic ligand is responsible for a characteristic band in the ultraviolet region, around 260 nm, ascribed to $\pi \rightarrow \pi^*$ transitions in the aromatic ring. Another band, of intermediate energy, is strongly sensitive to the oxidation states, as well as to the nature of the axial ligands, moving from 310 nm in the $Ru_3^{IV,III,III}O$ complex up to 800 nm in the completely reduced $Ru_3^{II,II,II}O$ form of the pyrazine complex, accompanied by a

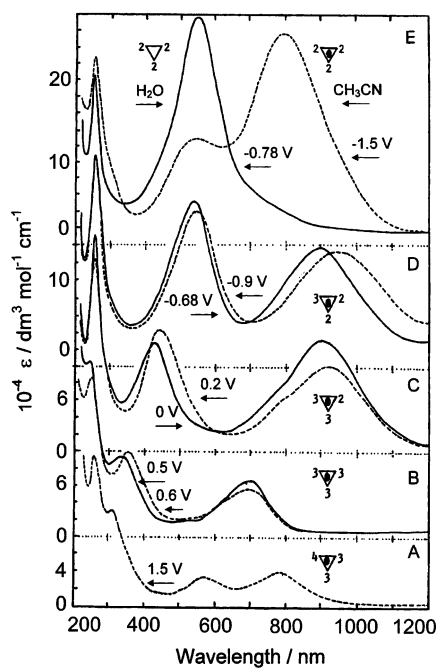

Fig. 5. Spectroelectrochemical behavior of the $[Ru_3O(Ac)_6(pz)_3]$ cluster in acetonitrile (- - -) and aqueous solution (—) at several applied potential (V vs. SHE). [KCl] = 0.1 M (H_2O) or $[NEt_4ClO_4]$ = 0.1 M (CH_3CN).

dramatic increase of intensity. This band exhibits a remarkable, selective resonance Raman effect for most totally symmetric pyrazine vibrational modes [21], supporting a charge-transfer transition from the occupied Ru^{II} d_{π} orbitals, e.g. of e″ symmetry, to the lowest unoccupied π* orbitals of the axial ligands.

Another interesting aspect is observed for the electrochemical and spectroelectrochemical behavior of the $[Ru_3O(Ac)_6(pz)_3]$ complexes in aqueous solution [67]. Only the waves associated with the $Ru_3^{III,III,III}O/Ru_3^{III,III,II}O/Ru_3^{III,II,II}O$ redox couples are accessible in aqueous solution, using gold or glassy carbon electrodes. Above pH 10, the two waves are typically reversible, with $E_{1/2} = 0.39$ and -0.65 V, respectively. The reduction of the $Ru_3^{III,III,III}O$ cluster is pH-dependent. Below pH 5, the redox wave moves to less negative potentials and becomes broader. At pH 3, the net charge involved is twice that observed at pH 10, being consistent with the transfer of two electrons, in a successive way, involving an intermediate proton-dependent step. In the reverse potential scan, the cathodic signal at -0.6 V exhibits a corresponding anodic peak at about -0.5 V, followed by another one at -0.1 V, regenerating the starting oxo-bridged $Ru_3^{III,III,II}O$ complex.

Spencer and Wilkinson [2] have shown that the $[Ru_3O(Ac)_6(py)_3]^+$ cluster can be reduced by hydrogen at 2 atm. pressure, in aqueous solution, in the presence of platinum oxide catalyst, yielding the corresponding $Ru_3^{II,II,II}$ end product with loss of the central μ-oxo ion. This species can be oxidized in a reversible way, without changing the overall structure of the triangular cluster. Based on the reversible behavior observed in acetonitrile solutions, and considering the results reported by Spencer and Wilkinson [2,20], the pH-dependent step observed in aqueous solution has been ascribed to elimination of the central oxygen ion in the $Ru_3^{II,II,II}O$ species. Above pH 10, such species is stable; however, at low pH, the transfer of the central oxygen ion to the solvent is facilitated, leading to a $Ru_3^{III,II,II}$ intermediate which undergoes further reduction to the $Ru_3^{II,II,II}$ end product, as shown in Scheme 2 [67].

The proposed mechanism has been confirmed from spectroelectrochemical measurements [67] carried out in aqueous solution. As shown in Fig. 6, the spectroelectrochemical behavior associated with the $Ru_3^{III,III,III}O/Ru_3^{III,III,II}O$ redox couple is typically reversible, with $E° = 0.40$ V. The spectral changes are very similar to those observed in acetonitrile solutions, showing a decay of the 340 and 705 nm bands,

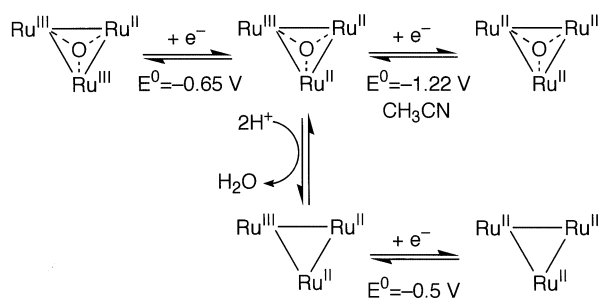

Scheme 2.

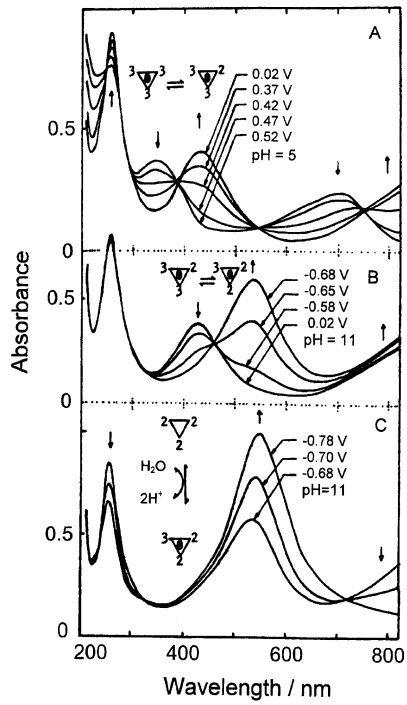

Fig. 6. Spectroelectrochemical behavior of the $[Ru_3O(Ac)_6(pz)_3]$ cluster aqueous solution at several applied potentials (V vs. SHE; [KCl] = 0.1 M): (A) reduction of $Ru^{III}Ru^{III}Ru^{III}$, pH 5; (B) reduction of $Ru^{III}Ru^{III}Ru^{II}$, pH 11; (C) formation of $Ru^{II}Ru^{II}Ru^{II}$ with loss of the central oxygen ion, pH 11.

and the rise of the 420 and 905 nm bands characteristic of the $Ru_3^{III,III,II}O$ complex. At pH > 10, the reduction of the $Ru^{III,III,II}$ cluster proceeds reversible with $E_{1/2} = -0.65$ V, shifting the visible charge-transfer band from 420 to 535 nm while the intracluster band at 885 nm becomes broader and more intense. The spectral changes are also very similar to those observed in acetonitrile solutions, indicating that the central oxygen bridge remains intact. However, below -0.68 V there is a systematic increase in the absorption band at 535 nm, and the intracluster band in the near-infrared region disappears, indicating that the d_π levels are saturated, as expected for the $Ru_3^{II,II,II}$ oxidation state. The final electronic spectrum does not coincide with that of the $Ru_3^{II,II,II}O$ species measured in acetonitrile. At pH < 5, within the time scale of the spectroelectrochemical measurements, the $Ru_3^{II,II,II}O$ species does not accumulate, converting rapidly into the $Ru_3^{II,II,II}$ end product, after the transfer of the central oxygen ion to the solvent. A partial loss of the oxygen bridging ion from the trinuclear cluster is also evident in the spectroelectrochemical measurements in acetonitrile solutions, due to the presence of trace amounts of water, as indicated by the presence of a shoulder around 550 nm.

An important conclusion from these results is that the central oxygen ion plays a key role in stabilizing Ru^{III} or Ru^{IV} species, by donating π-electrons to the empty

d_{yz} orbitals. When the cluster is in the $Ru_3^{II,II,II}$ form, the d_{yz} orbitals are saturated and this type of interaction is no longer possible, facilitating the transfer of the oxygen ion to the proton donor species in the solvent.

The oxidation states of the cluster can also have a determining role in the binding modes of the axial ligands. For instance, an electrochemically driven linkage isomerization has been reported for the dimethyl sulfoxide (dmso) complex [31], $[Ru_3O(Ac)_6(py)_2(dmso)]^+$. In this complex, according to the vibrational spectra, the dmso ligand is coordinated to the ruthenium center by means of the O atom, i.e. $Ru_3^{III,III,III}O$ ($\kappa O\{dmso\}$), where κ denotes the binding atom. Cyclic voltammograms have been measured in acetonitrile solutions, in the presence of a high excess of the dmso ligand, in order to prevent its dissociation from the complex. In this case, by starting from the $Ru_3^{III,III,III}O$ ($\kappa O\{dmso\}$) complex at 0.8 V, and scanning the potential in the direction of negative potentials, a single cathodic peak has been observed at $E_{1/2} = 0.13$ V, corresponding to the formation of the $Ru_3^{III,III,II}O$ ($\kappa O\{dmso\}$) species. In the reverse scan, in addition to the corresponding oxidation peak, another peak appears at $E_{1/2} = 0.42$ V, associated with the $Ru_3^{III,III,II}O$ ($\kappa S\{dmso\}$) isomer. By starting from the reduced complex at -0.5 V, the relative intensities of the pair of waves at 0.13 and 0.42 V are inverted, indicating that the $Ru_3^{III,III,II}O$ ($\kappa S\{dmso\}$) isomer predominates over the $Ru_3^{III,III,II}O$ ($\kappa O\{dmso\}$) one. This system can be treated in terms of the square scheme and the Nicholson and Shain procedure [70], in order to determine the equilibrium and kinetic isomerization constants, as shown below:

$$\begin{array}{ccc} [Ru_3{}^{III,III,III}O\ (\kappa O\{dmso\}) & \rightleftharpoons & [Ru_3{}^{III,III,III}O\ (\kappa S\{dmso\}) \quad (k^{III}{}_{S\rightarrow O}, k^{III}{}_{O\rightarrow S}) \\ \Downarrow\ E = 0.13\ V & & \Downarrow\ E = 0.42\ V \\ [Ru_3{}^{III,III,II}O\ (\kappa O\{dmso\}) & \rightleftharpoons & [Ru_3{}^{III,III,II}O\ (\kappa S\{dmso\}) \quad (k^{II}{}_{S\rightarrow O}, k^{II}{}_{O\rightarrow S}) \end{array}$$

where $k^{III}_{S\rightarrow O} = 1.2 \times 10^{-5}\ s^{-1}$, $k^{III}_{O\rightarrow S} = 1.5 \times 10^{-1}\ s^{-1}$, and $K^{III}_{O\rightarrow S} = 8.1 \times 10^{-5}\ s^{-1}$; $k^{II}_{S\rightarrow O} = 1.5\ s^{-1}$, $k^{III}_{O\rightarrow S} = 2.3 \times 10^{-1}\ s^{-1}$, and $K^{II}_{O\rightarrow S} = 6.5\ s^{-1}$.

The reaction rates for the oxidized and reduced clusters are much faster than the usual rates of substitution reactions, indicating an intramolecular linkage isomerization mechanism.

Redox-active ligands such as the *N*-methyl-4-4′-bipyridinium ions ($mbpy^+$) have also been employed [17,28], in a series of $[Ru_3O(Ac)_6(mbpy)_3]^{4+}$ and $[Ru_3O(Ac)_6(mbpy)_2L]^{2+}$ (L = CO, H_2O, pyrazine, pyridine, imidazole and 4-{dimethylamino}pyridine) complexes. In addition to the waves clearly assignable to the Ru_3O core-based processes, a splitting of the $mbpy^+$ ligand-based processes has been detected at variable extent, depending on the nature of L. The splitting of each ligand-based redox processes ($mbpy^{+/0}$, $mbpy^{0/-}$) into two one-electron steps indicates that electronic interactions between two terminal ligands can effectively occur through the triruthenium cluster core.

2.5. Properties and catalytic activity

The oxo-bridged trinuclear ruthenium clusters has been immobilized at modified silica gel [29], polypyrrol [23], poly(4-vinilpyridine) [71], and Prussian blue surfaces [72], keeping their original spectral and redox characteristics, for applications in catalysis and electrochromic devices. Recently, a novel species containing a disulfide alkyl ligand has been reported [44]. This cluster form monolayer assemblies on gold electrodes, exhibiting anion-depend redox behavior in aqueous solution.

The catalytic activity of oxo-bridged trinuclear ruthenium clusters in the hydrogenation of unsaturated hydrocarbons has been reported by Wilkinson and coworkers [73,74] and by Fouda et al. [75]. Similar studies have also been carried out for $[Ru_3O(Ac)_6(H_2O)_3]^+$ species [76] immobilized in a polymeric matrix. Intramolecular and intermolecular hydrogen transfer efficiencies have been evaluated for a number of ruthenium catalysts [77,78]. The $[Ru_3O(Ac)_6(H_2O)_3]^+$ cluster leads to the conversion of 1-hexene-3-ol to 3-hexanone at 98% yield, within 30 min, while the reference catalyst $[RuHCl(PPh_3)_3]$ required 1 h to reach 92% yield, under identical conditions. Efficient conversion of acrylonitrile to propionitrile and 1,4-dicyano-1,3-butadiene has also been reported for the $[Ru_3O(Ac)_6(H_2O)_3]^+$ complex [79]. A selective catalytic activity has been reported for the $[Ru_3O(Ac)_6(H_2O)_3]^+$ cluster in the reaction of butadiene with formaldehyde and acetic acid [80], yielding $CH_2CHCH(Ac)CH_2CH_2OH$ in 59% yield.

The oxo-bridged trinuclear ruthenium clusters can also promote efficient oxidation of olefins [81,82] and phenols [83] with hydroperoxides, providing a promising route for the preparation of 2,3,6-trimethylbenzoquinone, a key intermediate for the synthesis of vitamin E. Oxidation of primary and secondary alcohols using O_2 in the presence of $[Ru_3O(RCO_2)_6L_3]^n$ species ($R = CH_3$, C_2H_5; $L = H_2O$, PPh_3, $n = 0$, 1) [41] has also been reported. The observed selectivity is comparable to that for $RuCl_3 \cdot nH_2O$ or $RuCl_2(PPh_3)_3$, however, the catalytic activity is ten times higher. Several recent studies have been focused on the oxidation of olefins or cycloalkanes by O_2 in the presence of $[Ru_3O(pfb)_6(Et_2O)]pfb$ where pfb, $CF_3CF_2CF_2CO_2^-$ [6,51,84]. The catalytic activity of the ruthenium clusters immobilized in a polyethylene matrix containing functionalized carboxylate groups [56,85], has also been investigated. Polypyrrole films containing imobilized ruthenium clusters have been employed for the electrochemical oxidation of benzilic alcohol yielding benzaldehyde, with 46% yield [23].

3. Ligand-bridged dimers

Ligand-bridged cluster dimers such $[(py)_2Ru_3O(Ac)_6(BL)Ru_3O(Ac)_6(py)_2]^{2+}$ (where, BL, pyrazine, 4,4′-bipyridine-*trans*-1,2-bis(4-pyridyl)ethene and 1,2-bis(4-pyridyl)ethane bridging ligands) have been reported by Baumann et al. [86]. Their synthesis have been carried out by exploiting the lability of the methanol group in $[Ru_3O(Ac)_6(py)_2(MeOH)]^+$ and the binding properties of the bridging ligand (Scheme 3).

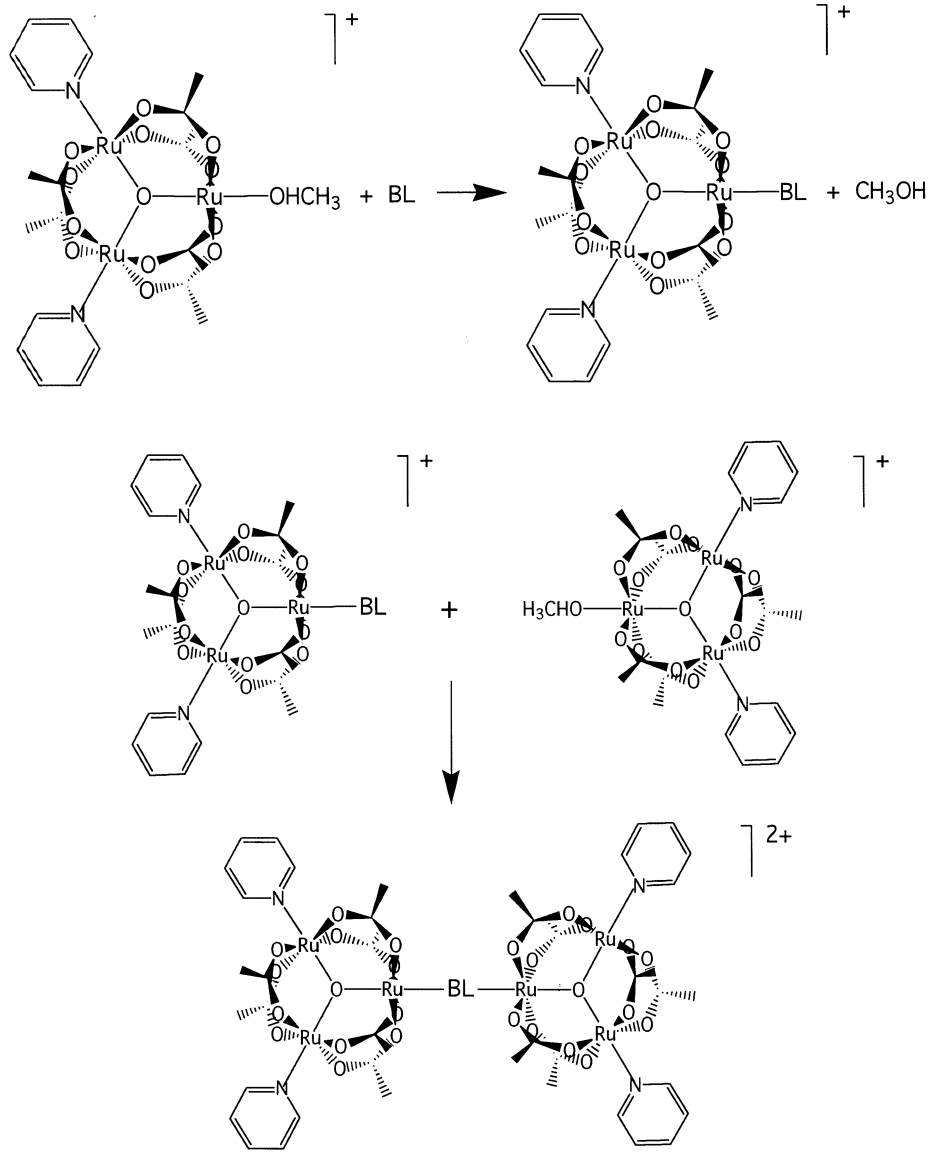

Scheme 3.

The dimers in the oxidized and reduced forms, including the ''mixed-valence'' species, can be readily obtained chemically or electrochemically. In addition to the typically reversible redox chemistry of the individual cluster moieties, the electrochemical behavior of the dimers also reflects the extent of intercluster interaction through the bridging ligands. The intercluster electronic interaction depends both on the bridging ligand and on the electronic density on the Ru_3O core. It seems

particularly strong in the case of the pyrazine dimer, because of the favorable overlap between the Ru_3O cluster d-orbitals and bridging π^*-orbitals. The intracluster electronic coupling increases as the complex is reduced, leading to the splitting of the cyclic voltammogram waves at $+0.33$ and 0.23 V ($\Delta E = 10$ mV) and at -0.86 and -1.13 V ($\Delta E = 270$ mV). These processes correspond to the successive monoelectronic reduction of the $[Ru_3^{III,III,III}O–pz–Ru_3^{III,III,III}O]$ and $[Ru_3^{III,III,II}O–pz–Ru_3^{III,III,II}O]$ species, respectively. In addition, a weak intercluster (intervalence) transition, has been suggested, in the near-infrared region (1000–1300 nm), for the $[Ru_3^{III,III,III}O–pz–Ru_3^{III,III,II}O]$ species. For the remaining BL ligands, the electronic coupling is much weaker, and in the corresponding "mixed-valence" species each cluster moiety seems to be independent, as in a valence localized system.

The rates of intramolecular electron transfer in this type of pyrazine-bridged dimeric mixed-valence clusters have been recently investigated by Ito and co-workers [33,36,48] based on the analysis of vibrational peak profiles. Carbon monoxide has been used as a suitable peripheral ligand in the cluster moiety, acting as an infrared vibrational probe. In addition, as indicated in Scheme 4, substituted pyridine ligands such as 1-azabicyclo[2,2,2]octane (abco) [36], 4-dimethylaminopyridine (dmap), pyridine and 4-cyanopyridine (cpy) have been employed as electron donor–acceptor groups, influencing the extent of electronic delocalization in the mixed-valence dimer.

Analogous to the $[(py)_2Ru_3O(Ac)_6(pz)Ru_3O(Ac)_6(py)_2]^-$ dimer, in the carbonyl analogues, $[(CO)L(Ac)_6Ru_3O(pz)Ru_3O(Ac)_6L(CO)]^-$, the reduction of the two $Ru_3^{III,III,II}O$ moieties proceeds in two steps, e.g. at -0.60 and -1.07 V; -0.65 and -1.09; -0.57 and -0.95; -0.44 and -0.69 V, for L, abco, dmap, py and cpy derivatives, respectively. The splitting of the reduction wave corresponding to the formal $[Ru_3^{III,III,II}O–pz–Ru_3^{III,III,II}O]/[Ru_3^{III,III,II}O–pz–Ru_3^{III,II,II}O]$ successive redox processes decreases from $\Delta E_{1/2} = 470$ to 250 mV,

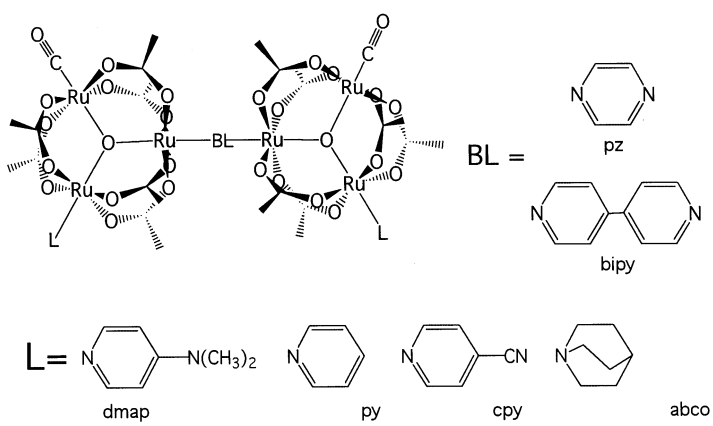

Scheme 4.

along the abco to cpy series. The $\Delta E_{1/2}$ values are related to the comproportionation equilibrium, K_c, for the reaction

$$[Ru_3^{III,III,II}O\text{-pz-}Ru_3^{III,III,II}O] + [Ru_3^{III,II,II}O\text{-pz-}Ru_3^{III,II,II}O] \rightleftharpoons [Ru_3^{III,III,II}O\text{-pz-}Ru_3^{III,II,II}O]$$

The comproportionation constants, K_c, vary from 9×10^7 to 1.7×10^4 along the series. In addition to the favorable overlap between the Ru_3O and the pyrazine π-orbitals, these results show that the intercluster electronic coupling can be controlled by the peripheral ligands, according to their ability to raise or lower the ruthenium cluster levels with respect to that of the bridging ligand.

In the mixed-valence species $[Ru_3^{III,III,II}O\text{–pz–}Ru_3^{III,II,II}O]$ an electronic band observed in the range of 800–925 nm has been ascribed to an intercluster charge-transfer transition. Estimates of the electronic coupling parameter, H_{AB}, derived from the corresponding optical data ranged from 2490 (abco) to 1310 cm^{-1} (cpy), supporting a delocalized class III behavior, according to the Robin–Day classification of intervalence charge-transfer complexes [87].

The vibrational spectra of the $[(CO)(dmap)(Ac)_6Ru_3O(pz)Ru_3O(Ac)_6(dmap)(CO)]^n$ dimer exhibit a single ν(CO) band at 1938 cm^{-1} for $n = 0$ and at 1889 cm^{-1} for $n = -2$. In the case of the mixed-valence dimer ($n = -1$) a broad absorption band at the average energy of the bands for $n = 0$ and $n = -2$ has been observed. In all the series of complexes, instead of the two ν(CO) peaks expected for the case of two non-equivalent centers, a coalescence behavior has been observed in the IR spectra, proportional to the degree of intercluster electronic coupling, H_{AB}. The dependence of IR absorption band-shape on electronic coupling in the mixed-valence states is consistent with extremely rapid intramolecular electron transfer, approaching the vibrational time scale. From spectral simulations based on infrared line shape calculations, electron transfer rates of 1×10^{12} and 5×10^{11} s^{-1} have been calculated for the abco and py complexes.

The study of the $[(CO)L(Ac)_6Ru_3O(pz)Ru_3O(Ac)_6L(CO)]^n$ complexes, has been extended to the less strongly coupled $[(CO)L(Ac)_6Ru_3O(bipy)Ru_3O(Ac)_6L(CO)]^n$ series containing the 4,4′-bipyridine bridging ligand [48] (Scheme 4).

As predicted, the observed splittings in the cyclic voltammograms involving the $n = 0$, -1 and -2 species were much smaller, i.e. $\Delta E_{1/2} = 120$, 80 and < 50 mV, for L = dmap, py and cpy, respectively. In contrast to the pyrazine analogues, the detection of the intercluster charge-transfer transitions has not been successful, presumably because of their small intensities, indicating a less-strongly coupled system. The infrared spectral behavior for ν(CO) are typical of valence localized systems, exhibiting essentially a single vibrational peak for each of the $n = 0$ and -2 species, with no evidence of coalescence for $n = -1$. The rate constants for intercluster electron transfer in the mixed-valence dimers were estimated to be below 10^{11} s^{-1}. Related studies have been recently reported for pyrazine-bridged cluster dimers containing terminal isocyanide ligands (CNXy) instead of carbon monoxide, as well as, for analogous 1,4-phenylene diisocyanide-bridged dimers [35].

4. Ligand-bridged trimeric clusters

Ligand-bridged trimeric clusters (Scheme 5) have been conveniently prepared [26] from the mononuclear species $[Ru_3O(Ac)_6(MeOH)_2(CO)]$, containing two labile methanol ligands, in the presence of the complementary species, e.g. $[(py)_2(Ac)_6Ru_3O(pz)]^+$.

The trimeric cluster $[\{(py)_2(Ac)_6Ru_3O(pz)\}_2\ Ru_3O(Ac)_6(CO)]^+$ has been considered as an "electron sponge" in terms of the extent of its multiple electron transfer behavior. In fact, a series of ten redox waves has been detected in the potential region from $+2.44$ to -1.47 V. By analogy with the corresponding monomeric analogues [3], the redox waves associated with the $(py)_2(Ac)_6Ru_3O(pz)$ moiety have been assigned at 2.29, 1.30, 0.28 V, corresponding to the $Ru_3^{IV,IV,III}O/Ru_3^{IV,III,III}O/Ru_3^{III,III,III}O/Ru_3^{III,III,II}O$ redox couples; while the redox waves of the $(pz)_2Ru_3O(Ac)_6(CO)$ center have been assigned at 1.73, 0.96, involving the

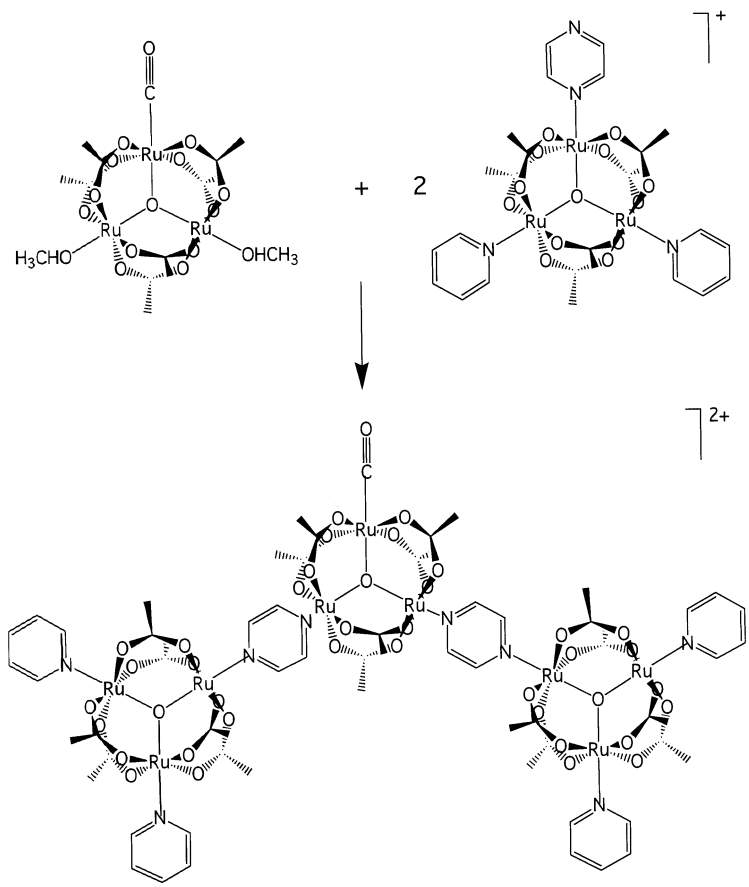

Scheme 5.

$Ru_3^{IV,III,III}O/Ru_3^{III,III,III}O/Ru_3^{III,III,II}O$ redox couples. The remaining waves at -0.39, -0.81, -0.97, -1.13, -1.32 V have been associated with the $Ru_3^{III,III,II}O/Ru_3^{III,II,II}O/Ru_3^{II,II,II}O$ redox couples in the central and peripheral clusters; however, the assignment becomes complicated by the splittings arising from the intercluster electronic interactions, as well as, by the concomitant reduction of the pyrazine ligand.

Another interesting approach has been employed by Kido et al. [32], for the synthesis of a trimeric pyrazine-bridged cluster, based on the $[Ru_3O(Ac)_6(py)(CO)(H_2O)]$ complex. This species exhibits a labile water molecule, which can be readily replaced by pyridine or pyrazine ligands. The carbonyl center is inert, but susceptible to photoelimination reactions, providing a second, selective substitution site. The pyridine ligand acts as an inert, non-reactive site. By reacting the $[Ru_3O(Ac)_6(py)_2(pz)]^+$ complex with the $[Ru_3O(Ac)_6(py)(CO)(H_2O)]$ species, a pyrazine-bridged dimeric cluster $[(py)_2(Ac)_6Ru_3O(pz)Ru_3O(Ac)_6(py)(CO)]^+$ has been generated. After irradiation for 2 h with a high pressure Hg lamp, the CO ligand is eliminated, yielding the corresponding substituted dimer exhibiting a labile MeOH site. The procedure has been repeated successfully, for the synthesis of the trimeric species, $[(py)_2(Ac)_6Ru_3O(pz)Ru_3O(Ac)_6(py)(pz)Ru_3O(Ac)_6(py)(CO)]^{2+}$ (Scheme 6).

5. Ligand-bridged tetrameric clusters

The synthesis of symmetric tetrameric clusters has been performed from the appropriate combination of the $[Ru_3O(Ac)_6(MeOH)_3]^+$ species with $[Ru_3O(Ac)_6(py)_2(BL)]^+$, in dichloromethane [38,39], where BL = pyrazine or 4,4′-bipyridine (Scheme 7). Their characterization is facilitated by the high D_{3h} symmetry, which can be readily checked using ^{1}H- and ^{13}C-NMR techniques. The contrasting spectra for the symmetric tetrameric species, and the related monomeric clusters, can be seen in Fig. 7.

In the case of the symmetric monomeric cluster $[Ru_3O(Ac)_6(4,4'\text{-bipy})_3]^+$, all the ligands are equivalent, leading to a sharp, strong peak at 5.09 ppm ascribed to the acetate protons, and four peaks at 0.63, 6.11, 7.13 and 8.54 ppm, ascribed to the 4,4′-bipyridine protons (see Fig. 7). The aromatic ligand protons, which are closer to the metal cluster, are readily distinguished by their large up field shifts in the resonance spectra, since they are strongly influenced by paramagnetic anisotropy effects, as well as by the inductive effects of the ruthenium ions [30]. The trinuclear cluster $[Ru_3O(Ac)_6(py)_2(4,4'\text{-bipy})]^+$ exhibits a C_{2v} symmetry, as shown in Fig. 7. The acetate protons appear as two sets of peaks at 4.96 and 5.07 ppm, reflecting the lowering in the symmetry. On the other hand, the occurrence of two peaks at 0.20 and 0.61 ppm reveals the existence of two types of ligand protons, located at the py and 4,4′-bipy ligands, close to the paramagnetic metal center.

For the tetrametric cluster $[Ru_3O(Ac)_6\{(4,4'\text{-bipy})Ru_3O(Ac)_6(py)_2\}_3]^{4+}$ there are distinct acetate protons, corresponding to the strongest peaks at 5.09, 4.96 and 4.84 ppm, respectively, in Fig. 7. The pyridine peaks are correlated with those observed

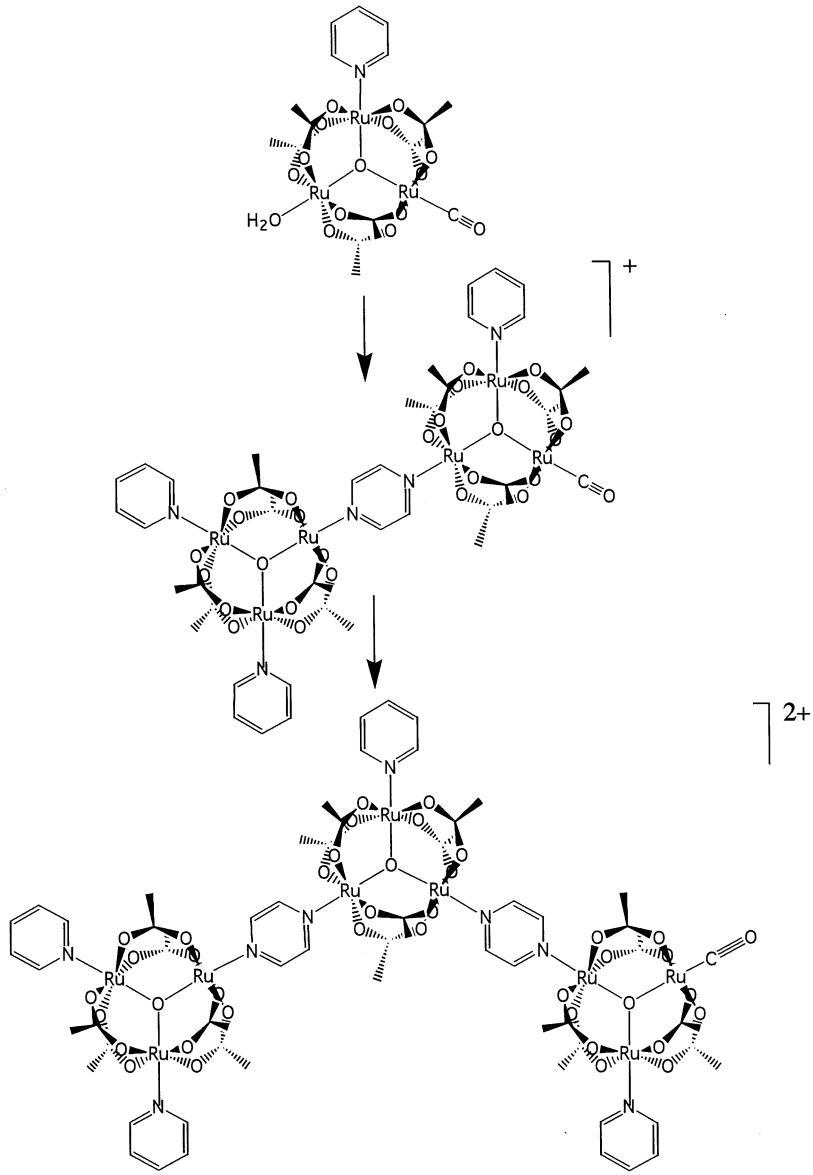

Scheme 6.

for the $[Ru_3O(Ac)_6(py)_2(4,4'\text{-bipy})]^+$ cluster. The resonance peaks for the bridging 4,4′-bipyridine ligand are expected to change more drastically, due to its double coordination to the paramagnetic ruthenium clusters. As a consequence, two distinct 4,4′-bipyridine signals appear in the high-field region, in addition to the pyridine peak.

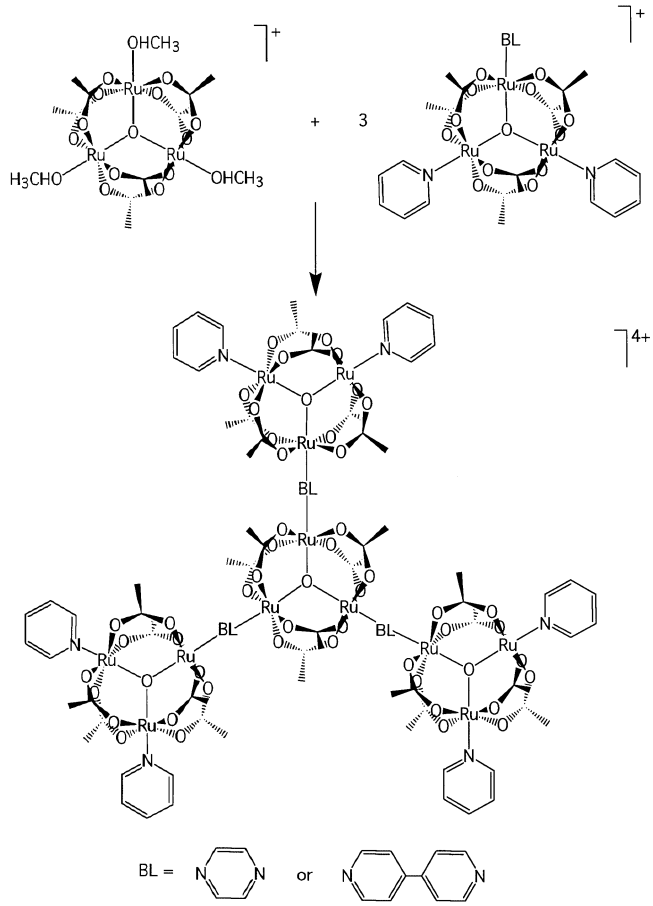

Scheme 7.

Analogous to the 4,4′-bipyridine species, the symmetric structure of the pyrazine-bridged tetrameric cluster $[Ru_3O(Ac)_6\{(pz)Ru_3O(Ac)_6(py)_2\}_3]^{4+}$ has also been proposed based on ^{1}H-NMR spectroscopy. Its electronic spectrum is very similar to the sum of the monomeric fragments contributions, exhibiting composite bands at 716, 616 and 514 nm ascribed to intracluster electronic transitions [39]. In addition, a cluster-to-pyrazine charge-transfer band at 420 nm and a cluster-to-pyridine charge-transfer band at 310 nm are observed in the spectrum. The most important difference in the spectra of the tetrameric and monomeric species is observed in the region of the cluster-to-pyrazine charge-transfer bands. For the monomeric cluster, $[Ru_3O(Ac)_6(py)_2(pz)]^{+}$, this band occurs at 370 nm, and the bathochromic shift to 420 nm in the tetrameric species reflects a significant electronic interaction through the cluster-pyrazine bond.

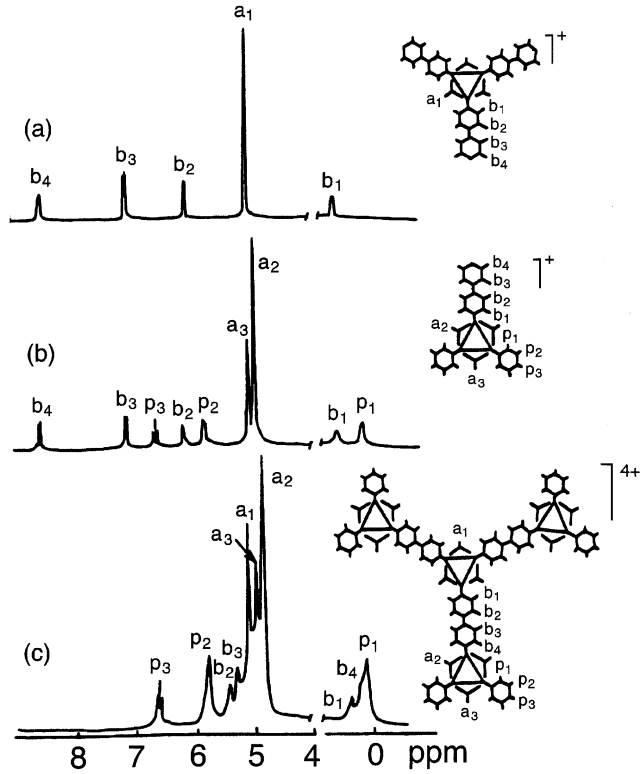

Fig. 7. ^{1}H-NMR spectra of the tetrameric species $[Ru_3O(Ac)_6\{Ru_3O(Ac)_6(py)_2(4,4'\text{-bpy})\}_3]^{+4}$ (c) and the related monomers (a) and (b) in CD_3CN solutions.

A comparison of the cyclic voltammograms for the $[Ru_3O(Ac)_6(py)_2(pz)]^+$ and the tetrameric cluster $[Ru_3O(Ac)_6\{(pz)Ru_3O(Ac)_6(py)_2\}_3]^{4+}$ can be seen in Fig. 8. The dodecanuclear cluster exhibits a strong, reversible wave at $E_{1/2} = 1.23$ V and a shoulder at 1.35 V involving the three peripheral and the central $Ru_3^{III,III,III}O$ clusters, respectively, generating the corresponding $Ru^{IV,III,III}$ species. The $E_{1/2}$ values for the $[Ru_3O(Ac)_6(py)_2(pz)]^{2+/+}$ and $[Ru_3O(Ac)_6(pz)_3]^{2+/+}$ clusters, i.e. 1.22 and 1.32 V are very close to the ones observed for the tetrameric species. The clusters undergo further oxidation to the corresponding $Ru_3^{IV,IV,III}O$ species, at 2.2 V. The reduction of the $Ru_3^{III,III,III}O$ dodecanuclear cluster to the $Ru_3^{III,III,II}O$ species proceeds according to two reversible steps at $E_{1/2} = 0.37$ and 0.22 V, ascribed to the central $[Ru_3O(Ac)_6(pz)_3]$ and peripheral $[Ru_3O(Ac)_6(py)_2(pz)]$ units, respectively. The corresponding $E_{1/2}$ values for the monomeric clusters, $[Ru_3O(Ac)_6(pz)_3]^{+/0}$ and $[Ru_3O(Ac)_6(py)_2(pz)]^{+/0}$ are 0.32 and 0.21 V, respectively. The next reduction process which converts the $Ru_3^{III,III,II}O$ species to the corresponding $Ru_3^{III,II,II}O$ oxidation state occurs in three steps, at $E_{1/2} = 0.71$, -0.99 and -1.16 V. The $E_{1/2}$ values for the isolated $[Ru_3(Ac)_6(pz)_3]$ and $[Ru_3O(Ac)_6(py)_2(pz)]$ clusters are -0.78 and -0.98 V, respectively. The occurrence of three peaks indicates that the

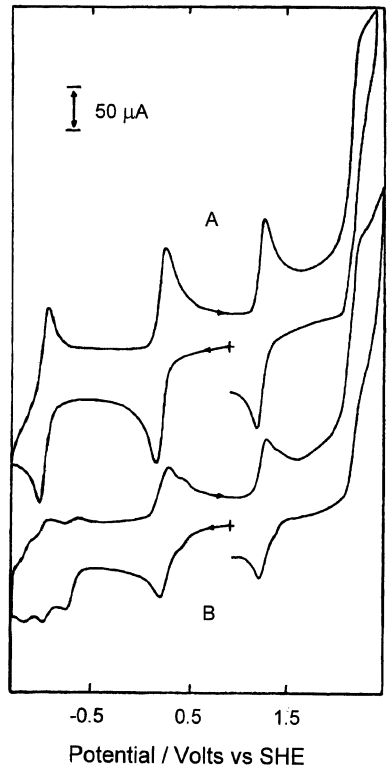

Fig. 8. Cyclic voltammogram of: (A) $[Ru_3O(Ac)_6(py)_2(pz)]^+$ (4.5 mM); and (B) $[Ru_3O(Ac)_6\{Ru_3O(Ac)_6(py)_2(pz)\}_3]^{+4}$ (1.1 mM) clusters in acetonitrile solutions, 0.1 M $TEAClO_4$.

reduction of the $[Ru_3O(Ac)_6(pz)_3]$ center at -0.71 V has a strong influence on the reduction of the peripheral $[Ru_3O(Ac)_6(py)_2(pz)]$ groups, splitting their corresponding waves by approximately 170 mV. As observed for the pyrazine-bridged dimeric and trimeric clusters, the splitting of the electrochemical waves is indicative of a strong intercluster electronic interaction via the pyrazine bridging ligands. Analogously, the degree of electronic coupling increases with the electron content of the oligomeric clusters.

6. Ligand-bridged cyclic polymeric clusters

A cyclic ligand-bridged polymeric cluster of composition $[Ru_3O(Ac)_6(CO)(pz)]_n$ has been isolated from the reaction of the $[Ru_3O(Ac)_6(CO)(MeOH)_2]$ complex with pyrazine, in methanol solution [42]. Its ^{1}H-NMR spectrum consists of a single pyrazine peak at 8.81 ppm, and two acetate signals at 2.29 and 2.13 ppm. The single pyrazine peak indicates unequivocally that all the pyrazine protons are equivalent, as in the case of a ligand-bridged symmetric polymer. On the other

hand, the observation of only two acetate protons with 1:2 intensity ratio indicates that all the trinuclear cluster moieties are equivalent, exhibiting axial microsymmetry. Therefore, the possibility of linear or non-cyclic structures has been ruled out.

The FTIR spectrum (Fig. 9) exhibits the peaks of the ruthenium cluster core at 1568 and 1423, ν(COO); 1348, $\delta(CH_3)$; and 623 cm^{-1}, π(COO); and the pyrazine vibrations at 1604 cm^{-1}, ν(CC); 1043, 943, 814, ν(CH ring); and 687 cm^{-1}, δ(ring). A single ν(CO) peak is observed at 1951 cm^{-1}, in complete agreement with a symmetric cyclic structure. The resonance Raman spectra exhibited the pyrazine vibrational peaks at 1603 cm^{-1}, ν(CC), 1226 ν(CH ring), 1036 ν(ring), 779 π(CH) ring, in addition to the clusters peaks at 667 cm^{-1}, π(COO); 447 ν(Ru–OCO) and 301 cm^{-1}, $\delta(Ru_3O)$. In this type of system, it has been shown that the most strongly enhanced vibrations in resonance Raman spectra correspond to totally symmetric modes [21,88].

Since the infrared active modes are anti-symmetric, the lack of coincidence between the FTIR and resonance Raman spectra confirms that the polymeric cluster has a center of symmetry. It is known [28] that the Ru_3O core has equilateral triangle geometry. When there is a CO molecule coordinated to the core, this geometry is slightly distorted, but the angles between the Ru and the central O atoms remain very close to 120°. The geometry of the triangular clusters strongly

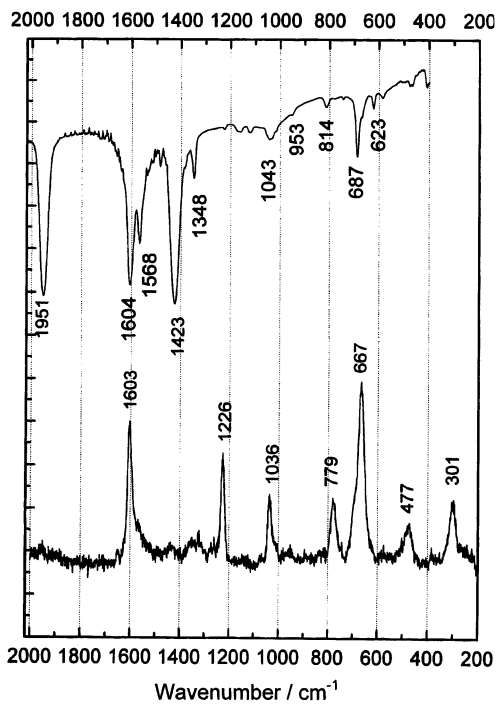

Fig. 9. Infrared (top) and resonance Raman (bottom) spectra of $[Ru_3O(Ac)_6(CO)(pz)]_6$, obtained in KBr pellet and solid sample, respectively.

favors the build up of a hexagonal structure, as shown in Scheme 8, in which each vertex of the hexamer is occupied by one $[Ru_3O(Ac)_6(CO)]$ unit. This expectation has been confirmed by molecular mechanics simulations, which indicated a preferential stabilization of the cyclic hexamer structure over all other possible spatial arrangements. This point also explains the self-assembly of the cyclic hexamer from the monomeric species.

The electronic spectrum of the hexamer (Fig. 10) shows two broad bands at 462 and 611 nm, ascribed to cluster-to-pyrazine charge-transfer and intracluster transitions, respectively. Both transitions are red shifted when compared to the same transitions for the monomeric cluster $[Ru_3O(Ac)_6(CO)(pz)_2]$, e.g. 406 and 593 nm, respectively [26]. The broadening of the electronic bands and the observed bathochromic shifts are consistent with the formation of extended structures, reflecting the π-electronic interactions through the cluster-pyrazine bond.

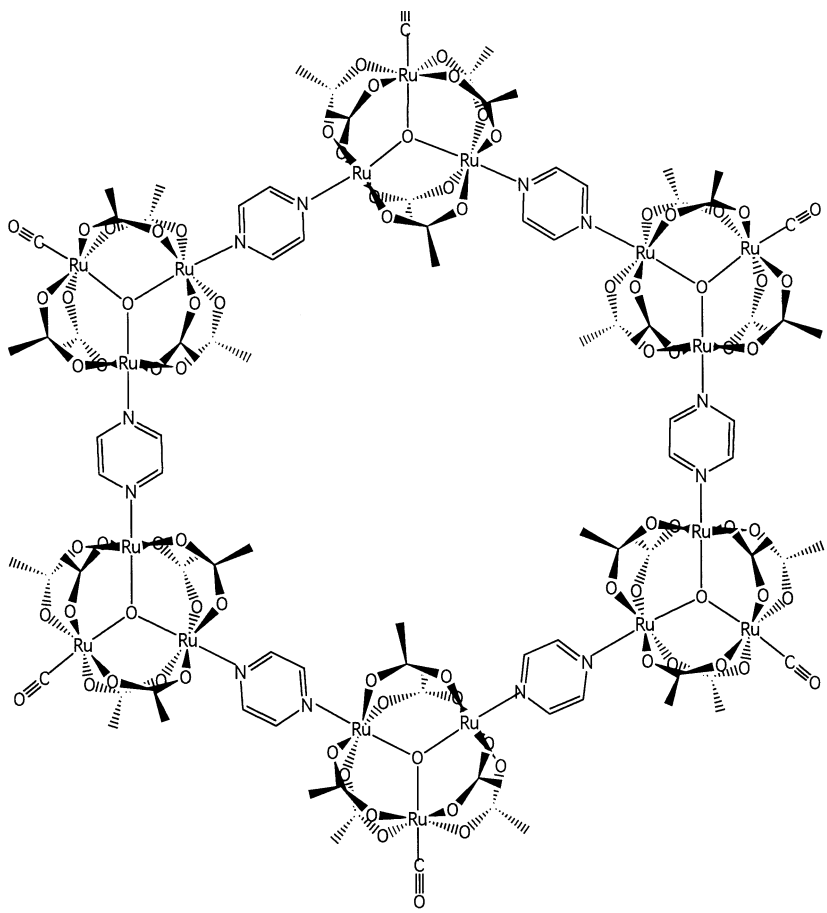

Scheme 8.

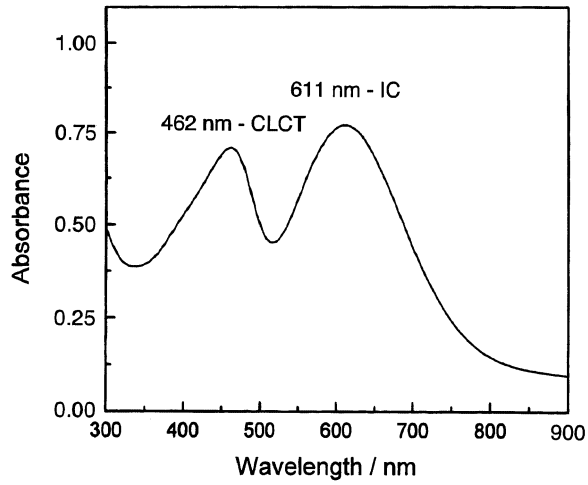

Fig. 10. Electronic spectrum of $[Ru_3O(Ac)_6(CO)(pz)]_6$, obtained from a 2.85×10^{-5} M CH_3CN solution (IC, intra-cluster; and CLCT, cluster-to-ligand charge-transfer transitions).

7. Mixed polynuclear clusters

The use of bridging ligands such as pz and 4,4′-bipy, coordinated to the $[Ru_3O(Ac)_6]^n$ core provides an effective template for building up mixed polynuclear cluster complexes. The reported cases have been inspired on related polynuclear systems derived from tris(bipyrazine)ruthenium(II) [89–91], and involve the direct binding of pentaammineruthenium(II) or pentacyanoferrate(II) ions to the $[Ru_3O(Ac)_6(pz)_3]$ cluster [88], yielding symmetric hexanuclear species (Scheme 9).

The $[Ru_3O(Ac)_6\{(pz)Ru(NH_3)_5\}_3]^{6+}$ hexanuclear cluster exhibits a broad, composite absorption band at 1005 nm, ascribed to intracluster metal–metal transitions (Fig. 11). The binding of the three $[Ru(NH_3)_5]^{2+}$ complex gives rise to a bathochromic shift, as compared with the corresponding transitions in the $[Ru_3O(Ac)_6(pz)_3]$ complex, at 950 nm. Spectral deconvolution of the strong absorption band in the near infrared region has been consistent with three Gaussian components at 1005, 865 and 700 nm, ascribed to the symmetry allowed $e'' \rightarrow a_2''$ and $a_1' \rightarrow a_2''$, and to the $e'(1) \rightarrow a_2''$ electric dipole forbidden transitions in the Ru_3O center. Another strong absorption band has been observed at 533 nm (Fig. 11), corresponding to a metal-to-pyrazine charge-transfer transition. This type of band can be observed at 422 nm, in the $[Ru_3O(Ac)_6(pz)_3]$ complex. The bathochromic shift has been associated with the stabilization of the pyrazine π^* orbitals induced by the coordinated metal ions, while the great enhancement has been ascribed to the overlap with the metal-to-pyrazine charge-transfer transitions involving the peripheral pentaammineruthenium(II) moieties. The corresponding band in the pentaammine(pyrazine)ruthenium(II) complex has been observed at 472 nm [92].

The existence of two metal-to-pyrazine charge-transfer bands in the visible region has been confirmed by the corresponding resonance Raman excitation profiles.

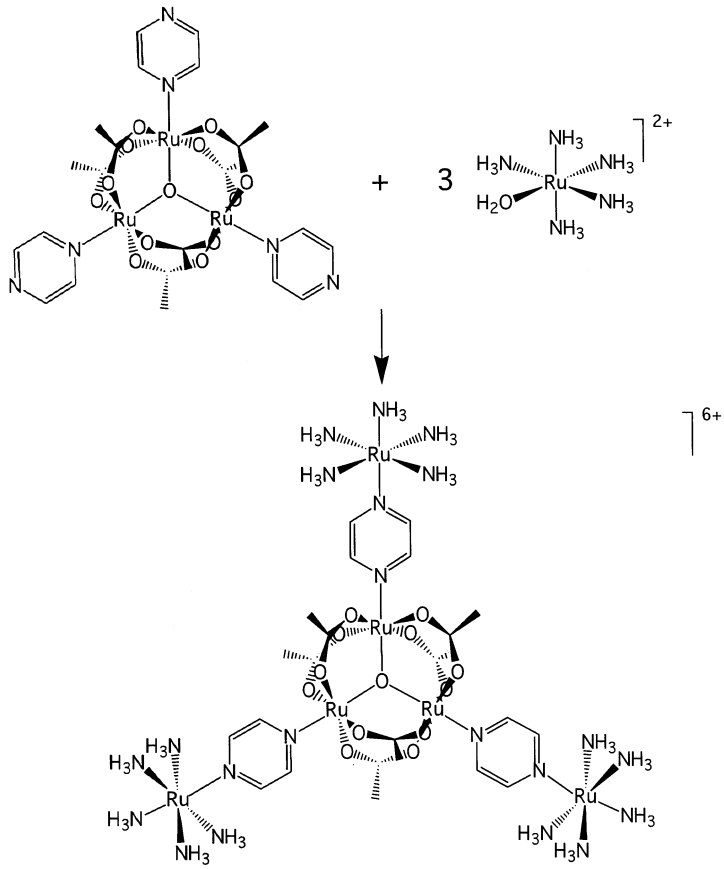

Scheme 9.

Optical excitation in the visible region induces a selective resonance Raman effect, enhancing the 1600, 1230 and 690 cm^{-1} vibrational peaks in the $[Ru_3O(Ac)_6(pz)_3]$ cluster, and the 1605, 1230, 1085, 695 cm^{-1} peaks in the $[Ru_3O(Ac)_6\{(pz)Ru(NH_3)_5\}_3]^{6+}$ species, associated with pyrazine vibrational peaks of a_1 symmetry. An additional peak at 335 cm^{-1} is strongly enhanced in the resonance Raman spectra of the hexanuclear cluster. This vibrational peak is not observed in the spectra of the trinuclear cluster, and has been ascribed to the $(NH_3)_5Ru–N(pz)$ stretching mode. The excitation profiles for the hexanuclear cluster, in the visible region, are rather asymmetric, particularly for the 335 cm^{-1} vibrational peak, indicating that the visible band is actually composed of overlapping cluster-to-pyrazine and pentaammineruthenium(II)-to-pyrazine charge-transfer transitions.

A related, symmetric hexanuclear cluster has been obtained from the reaction of the $[Ru_3O(Ac)_6(pz)_3]$ complex with pentacyanoferrate(II) ions [72]

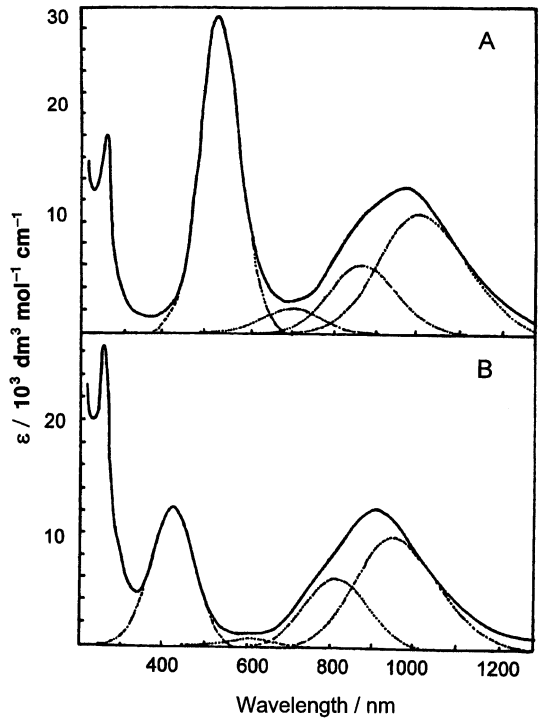

Fig. 11. Electronic spectra of: (A) hexanuclear cluster $[Ru_3O(Ac)_6(pz)_3\{Ru(NH_3)_5\}_3]^{+6}$; and (B) the monomeric cluster $[Ru_3O(Ac)_6(pz)_3]$ in aqueous solution (the Gaussian components from the deconvolution are represented under the bands).

$$[Ru_3O(Ac)_6(pz)_3] + 3[Fe(CN)_5H_2O]^{3-}$$
$$\rightarrow [Ru_3O(Ac)_6\{(pz)Fe(CN)_5\}_3]^{9-} + 3H_2O$$

The $[Fe(CN)_5H_2O]^{3-}$ ions react rapidly with the pyrazine ligands in $[Ru_3O(Ac)_6(pz)_3]$, yielding the 1:1, 1:2 and 1:3 substituted complexes. The reaction can be monitored spectrophotometrically by the rise of a strong absorption band at 520 nm, very similar to that reported for the $[Ru_3O(Ac)_6\{(pz)Ru(NH_3)_5\}_3]^{6+}$ species. The kinetic constants for the stepwise formation reactions were measured by the stopped-flow technique as $k_f = 50$, 42 and 15 $M^{-1}\,s^{-1}$, respectively. The complexes dissociate in the presence of a high excess of dimethyl sulfoxide, allowing the measurement of the corresponding dissociation constants, $k_d = 2.5 \times 10^{-4}$, 3.0×10^{-4} and $3.5 \times 10^{-4}\,s^{-1}$. From the kinetic constants, the equilibrium constants for the 1:1, 1:2 and 1:3 complexes were calculated as 2.5×10^5, 1.3×10^5 and 4.2×10^4 M^{-1}, respectively.

Cyclic voltammograms for the $[Ru_3O(Ac)_6\{(pz)Fe(CN)_5\}_3]^{9-}$ complex in aqueous solution, exhibited two reversible waves at 0.44 and 0.68 V, exhibiting relative intensities very close to 1:3. The first wave was ascribed to the $Ru_3^{III,III,III}O/Ru_3^{III,III,II}O$ redox couple, while the second one was ascribed to the $Fe^{III/II}$ redox

couple, by analogy with the series of substituted pentacyanoferrate(II) complexes [93]. The electrochemical behavior for this system has been consistent with polynuclear systems containing identical, weakly interacting redox groups. In this case, it has been shown [94] that the voltammograms exhibit the same shape as that obtained with the corresponding molecule containing a single center, but the magnitude of the current is enhanced by the presence of additional electroactive centers.

An interesting property of the $[Ru_3O(Ac)_6\{(pz)Fe(CN)_5\}_3]^{9-}$ complex is its ability to form stable films onto nickel surfaces, analogous to those reported for the hexacyanoferrate(II) ion and related hexacyanometallates [95–100]. The voltammograms of the immobilized films (Fig. 12) display some similarity with those obtained for the complex in solution, exhibiting a less intense wave at 0.47 V, ascribed to the ruthenium cluster, and a broad strong wave involving two components with $E° = 0.67$ and 0.76 V, associated with the $[Fe(CN)_5]^{3-}$ groups. The splitting of the iron–cyanide wave has been ascribed to non-equivalent structural sites in the films. The electrochemical response of this type of film is sensitive to the nature of the cations present in the supporting electrolyte. While potassium ions yield a sharp response, sodium and lithium ions lead to less intense and broad electrochemical waves. This result has been ascribed to the higher diffusion

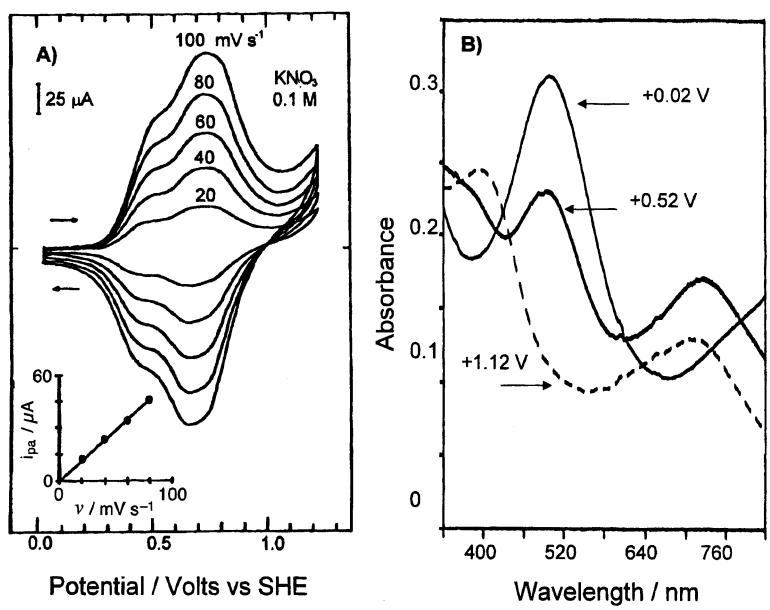

Fig. 12. Cyclic voltammograms of the $Ni_x[Ru_3O(Ac)_6(pz)_3\{Fe(CN)_5\}_3]_y$ modified electrode in aqueous solution, in the presence of $[KNO_3] = 0.1$ M (the inset shows the linear dependence of the anodic peak current vs. scan rates. (B) Spectroelectrochemical behavior of the ITO-$Ni_x[Ru_3O(Ac)_6(pz)_3\{Fe(CN)_5\}_3]_y$ modified electrode, in aqueous solution containing 0.5 M KCl at several applied potentials (vs. SHE). The electrode coverage is 1×10^{-9} mol cm^{-2}.

coefficient of the potassium ions, which are less hydrated and can migrate more rapidly through the polymeric films.

The electrochemical response of the $Ni_x[Ru_3O(Ac)_6\{(pz)Fe(CN)_5\}_3]_y$ films is rather reproducible. It is also accompanied by dramatic electrochromic effects, as shown in Fig. 12 (B), changing from violet (at 0 V), to gray (0.5 V) and green (1 V) during each cycle, reflecting the spectral changes associated with the several oxidation states of the hexanuclear cluster.

Another example of mixed polynuclear cluster has been provided by the $[Ru_3O(Ac)_6\{(ampz)Ru(edta)\}_3]^{4-}$ system, where ampz = 2-aminopyrazine [24]. This complex was generated in solution from the reaction of the $[Ru_3O(Ac)_6(ampz)_3]^{+}$ complex with $[Ru(edta)(H_2O)]^{2-}$ in high excess. The formation of the hexanuclear cluster was investigated using spectroelectrochemical and cyclic voltammetry techniques. The binding of $[Ru^{II}(edta)]^{2-}$ to the ampz ligands in the cluster proceeds rapidly in aqueous solution, and leads to the stepwise formation of multibridged complexes exhibiting strong metal-to-ligand charge-transfer bands at 530 nm. Their stability constants were around 10^4 M^{-1}.

An interesting ligand-bridged species was recently obtained by combining the $[Ru_3O(Ac)_6(py)_2(4,4'\text{-bipy})]^{+}$ complex with $[Ru(bipy)_2Cl]^{+}$ ions [43] (Fig. 13). This type of complex involves a photochemically active center, very close to a tunable redox-active species, constituting a prototype species for photoinduced electron transfer studies. A similar approach has been reported based on the combination of ruthenium clusters and porphyrins, involving very fast intramolecular electron transfer [101].

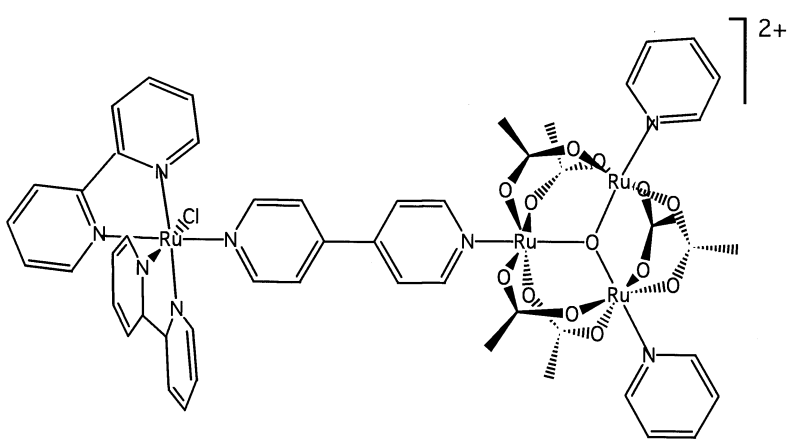

Fig. 13. Schematic structure of the $[Ru_3O(Ac)_6(py)_2(4,4'\text{-bpy})Ru(bpy)_2(Cl)](PF_6)_2$ dimer.

8. Polynuclear porphyrin–ruthenium clusters

Trinuclear ruthenium clusters and porphyrins provide a rather interesting combination to be exploited in supramolecular chemistry, particularly as models of biological catalysts [102–113] and in studies of electron transfer, artificial photosynthesis [110–112,114–117] and molecular devices [105,118–120]. Porphyrins and related species are extensively involved in the active sites of biological systems, displaying a wide range of catalytic properties. By attaching trinuclear ruthenium clusters to the porphyrin subunit their complementary role as electron carriers and redox-active sites can be conveniently exploited for the generation of supramolecular species exhibiting enhanced catalytic properties.

The chemical routes for binding trinuclear ruthenium clusters to *meso*-tetrapyridylporphyrins (TPyP) have been severely limited by solubility and stability problems. In fact, TPyP is rather insoluble in most conventional solvents. The use of high temperatures or more drastic conditions were attempted in the past, with little success, because the $[Ru_3O(Ac)_6L_3]^+$ clusters do not resist prolonged heating in solution. Only recently, a mild, convenient procedure has been reported, using trifluoroethanol as the solvent [121], for the synthesis of a tetracluster porphyrin, here denoted TCP (Fig. 14), as well as, its Zn, Mn and Co derivatives, i.e. ZnTCP, MnTCP and CoTCP, respectively.

These species are quite stable in the solid state, and are soluble in most of the conventional solvents, in contrast to the starting TPyP compound. Structural characterization in solution has been carried out by means of ^{1}H- and ^{13}C-NMR spectroscopy. The high symmetry (D_{4h}) of the molecule makes all related peripheral cluster resonances equivalent, and reduces the NMR spectrum of the TPyP center to a minimum set of peaks, thus providing reliable structural evidence for the tetrasubstituted species. A complete assignment [122] was published for ZnTCP, based on COSY, DEPT-135 and HETCOR experiments, as illustrated in Figs. 15 and 16.

The sharp singlet peak at 7.85 ppm for ZnTCP (Fig. 15) is not coupled with any other peak and its position and intensity is consistent with the eight equivalent pyrrole protons, in a D_{4h} symmetry. The two intense singlet peaks at 5.02 and 5.11 ppm also do not couple with any other protons in the molecule, but are characteristic of the methyl protons of the acetate ligands, in agreement with the proposed symmetric structure. It is known that the paramagnetic properties of the Ru_3O core can induce large up field shifts on the resonance frequencies of coordinated pyridine protons. This effect decreases rapidly as a function of distance, so that only the *ortho*-pyridyl protons are strongly shifted to 0.25 ppm, while the *meta*- and *para*-pyridyl signals are found at 5.82 and 6.58 ppm, respectively.

A comparison of the ^{1}H and ^{13}C chemical shifts for TCP and ZnTCP, is shown in Table 3. There is a good correspondence between the NMR signals for the two species. The CH_3 signals from the acetate groups are rather sensitive to changes in the nature and basicity of the axial *N*-heterocylic ligands [30,50]. A down field shift of the methyl groups signal in ZnTCP with respect to those for H_2TCP is observed. This indicates that the coordination of Zn^{II} leads to an enhancement of the acidity

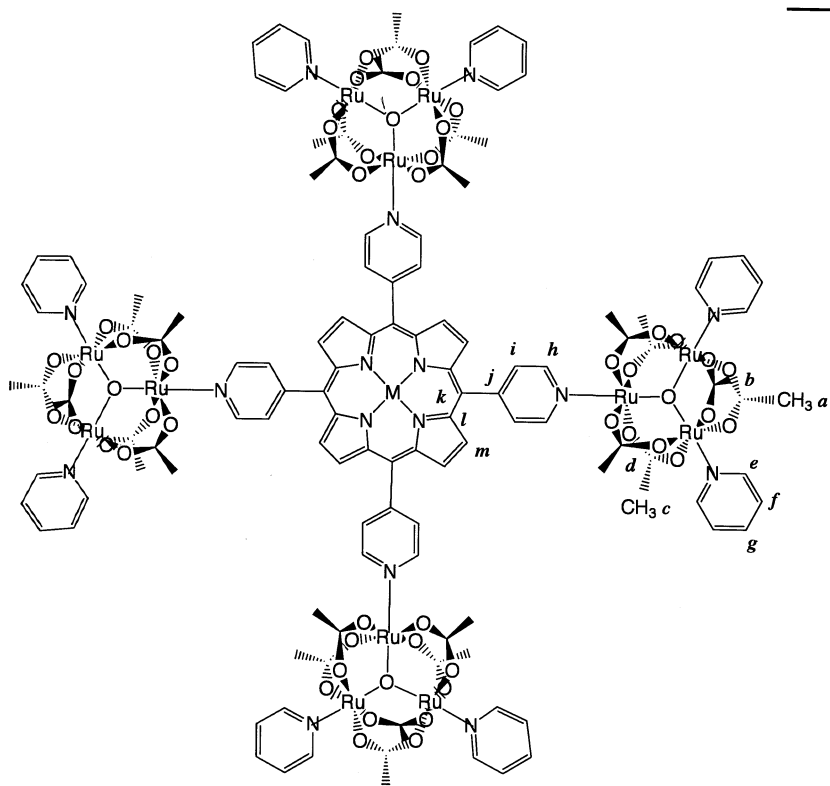

Fig. 14. Schematic structure of M-TCP (tetracluster porphyrin), where $M = 2H^{+}$, Zn^{2+}, Co^{3+} and Mn^{3+}.

of the porphyrin center, which propagates through the bridging pyridine ligands to the cluster units.

For the MnTCP and CoTCP species, the NMR spectra have also been reported, exhibiting additional features associated with the presence of paramagnetic anisotropy from the metal center, responsible for a significant broadening and shift of the neighboring protons signals to high frequencies.

The electronic spectrum of TCP in acetonitrile exhibits a continuous envelope of superimposed porphyrin and cluster bands from 200 to 800 nm. An illustrative spectral deconvolution has been carried out, as shown in Fig. 17, based on Gaussian analysis. The porphyrin Soret band is well defined at 414 nm and is followed by a high-energy vibronic shoulder at 382 nm. The deconvolution reveals four relatively narrow porphyrin Q bands at 518, 552, 579 and 654 nm, characteristic of the free-base porphyrin core, as well as, the characteristic intracluster metal–metal bands at 707, 604 and 508 nm. In the ultraviolet region there are two absorption bands at 237 and 274 nm ascribed to the $\pi \rightarrow \pi^{*}$ transitions in the

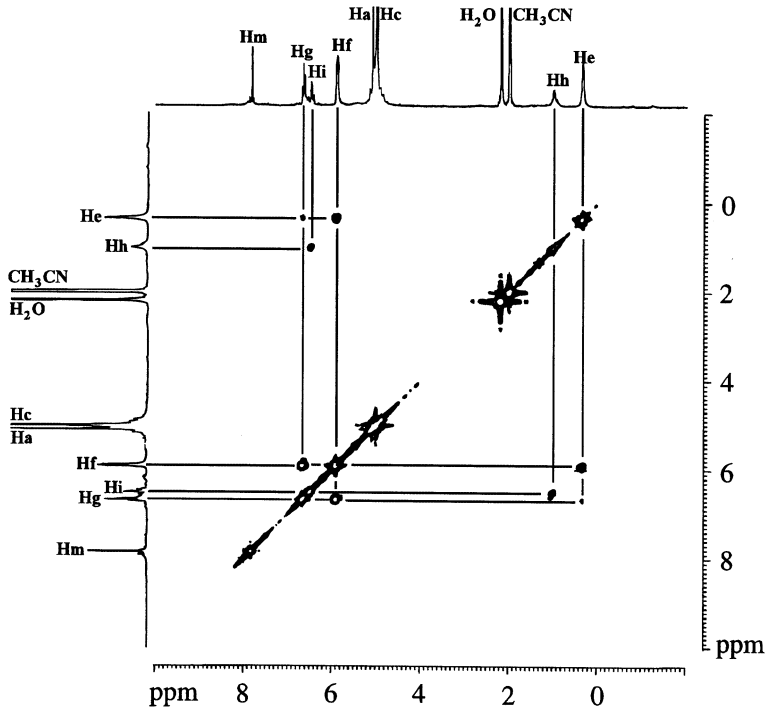

Fig. 15. Homonuclear $^{1}H,^{1}H$-COSY correlation spectrum of a 2×10^{-3} M solution of ZnTCP in CD_3CN.

terminal and bridging pyridine groups, respectively, while the next two bands at 314 and 351 nm fall in the region of weak porphyrin transitions overlapping with charge-transfer transitions from the metal cluster to the two types of pyridine ligands, as previously observed for $[Ru_3O(Ac)_6(py)_2(py–R)]^+$ complexes [38].

The electronic spectrum of the ZnTCP derivative is slightly less structured in comparison with that of TCP, since only two components of the Q band are observed at 572 and 619 nm, in agreement with the D_{4h} symmetry of the porphyrin center. The main intracluster band is observed at 685 nm, while the porphyrin Soret band occurs at 436 nm, in acetonitrile solutions. An interesting point is that the position of the Soret band is strongly sensitive to the presence of coordinating species, such as water, pyridine and imidazole, reflecting their direct interaction with the Zn^{II} center. In acetonitrile solutions, the corresponding binding constants have been measured as 1.6, 150 and 4000 M^{-1}, respectively; while in dichloromethane, the ligand affinity seems to increase by more than two orders of magnitude.

For the CoTCP species, the Soret and Q bands has been observed at 435 and 557, 611 nm, respectively. The main intracluster band is found at 693 nm. In the case of the MnTCP species, the Mn^{III}–porphyrin core is more strongly influenced

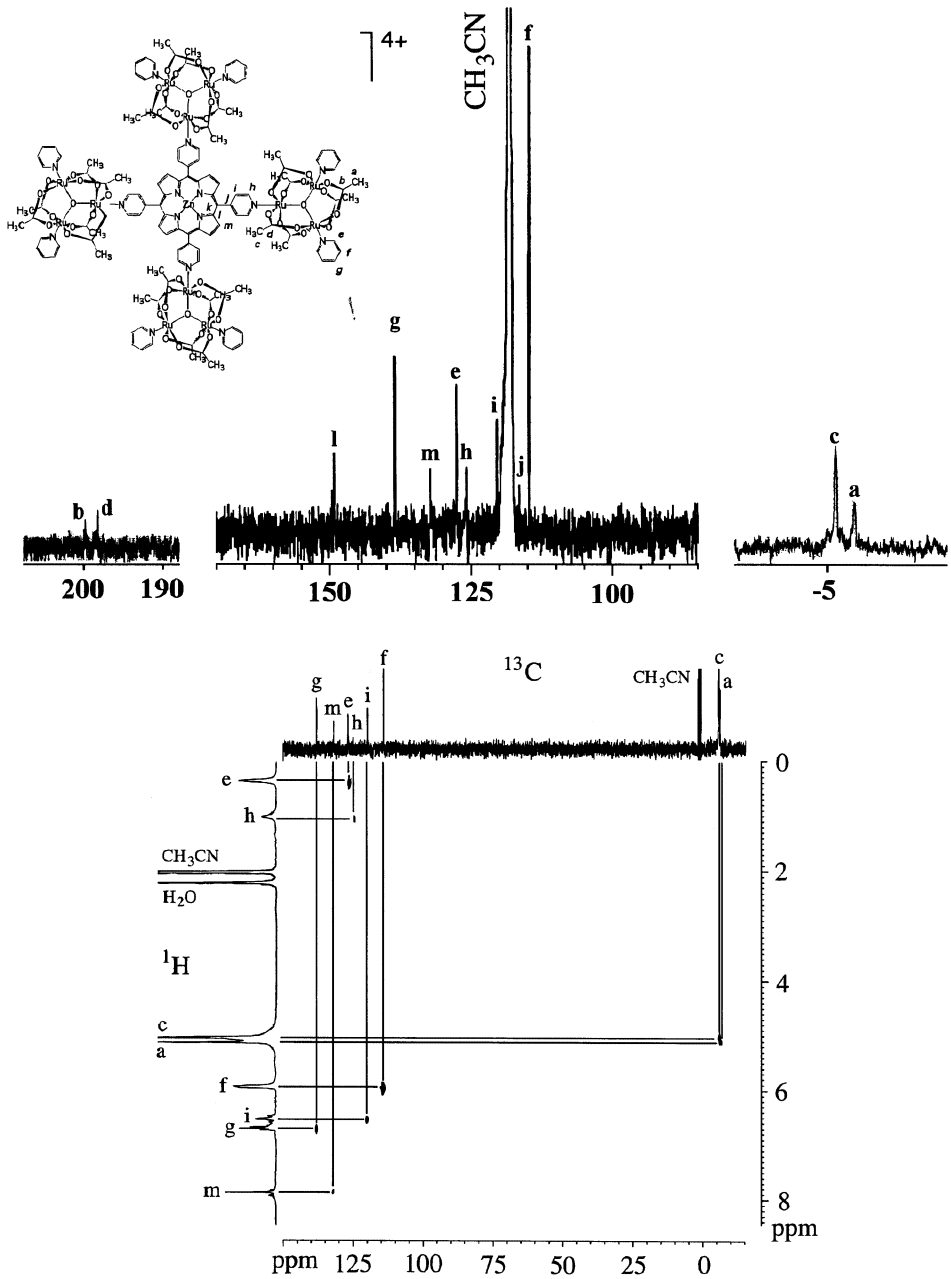

Fig. 16. ^{13}C-NMR and heteronuclear ^{1}H,^{13}C-HETCOR correlation spectrum of a 2×10^{-3} M solution of ZnTCP in CD_3CN.

Table 3
^{1}H and ^{13}C chemical shifts (δ, ppm) of a 2×10^{-3} M solution of ZnTCP in CD_3CN (see Fig. 14 for the nuclei labeling scheme)

Nuclei	^{1}H signals		^{13}C signals	
	ZnTCP	H_2TCP	ZnTCP	H_2TCP
a	5.11	4.57	−5.8	−2.9
b			199.8	203.2
c	5.02	4.49	−5.3	−3.5
d			198.3	199.2
e	0.34	0.73	127.6	113.8
f	5.92	6.13	114.7	119.3
g	6.69	6.63	138.5	131.5
h	1.00	0.03	125.9	115.0
I	6.52	6.63	120.4	138.3
j			Not observed	144.0
k			116.4	124.3
l			149.2	148.8
m	7.85	7.78	132.2	126.4

by the transition metal center as compared with the ZnTCP and CoTCP analogues. The Soret band (also referred as band V) is observed at 475 nm, in acetonitrile solutions, while the Q bands (or bands III and IV) occur at 621 and 584 nm. The main intracluster band is observed at 694 nm.

The cyclic voltammograms of the TCP complex (Fig. 18) are dominated by the peaks of the μ-oxo-ruthenium acetate cluster moieties, exhibiting four intense waves at 2.3, 1.23, 0.16 and −1.14 V ascribed to the successive redox couples $Ru_3^{IV,IV,III}O$/$Ru_3^{IV,III,III}O$/$Ru_3^{III,III,III}O$/$Ru_3^{III,III,II}O$/$Ru_3^{III,II,II}O$. The lack of splitting of the respective cluster waves indicates that the four peripheral units behave as independent redox sites, i.e. the cluster–cluster electronic coupling through the porphyrin bridge is negligible. The porphyrin subunit is also electrochemically active, giving rise to electrochemical waves at −0.72, −1.05, and 1.68 V, exhibiting intensities four times smaller than the waves associated with the ruthenium cluster. The two waves at −0.72 and −1.05 V are comparable to those observed at −0.68 and −0.93 V, for the analogous tetrapyridylporphyrin species modified with four $[Ru(bipy)_2Cl]^+$ groups, while the oxidation wave at 1.68 V is typically irreversible. The small shift ($\sim$50 mV) to more negative potentials is consistent with the π-backbonding interactions from the $Ru_3^{III,III,II}O$ clusters, which increase the electronic density of the porphyrin center.

The oxidation of the TCP species at 1.5 V is accompanied by a decrease of the intracluster bands in the 600–700 nm range, while a new absorption band appears at 826 nm, associated with $Ru_3^{IV,III,III}O$ moieties. This potential is at the onset of the porphyrin oxidation wave (1.68 V), and as a consequence, there is a systematic decay of the Soret band. At −0.3 V, a reversible reduction of the cluster centers to the $Ru_3^{III,III,II}O$ state can be observed from the decrease of the intensity of the

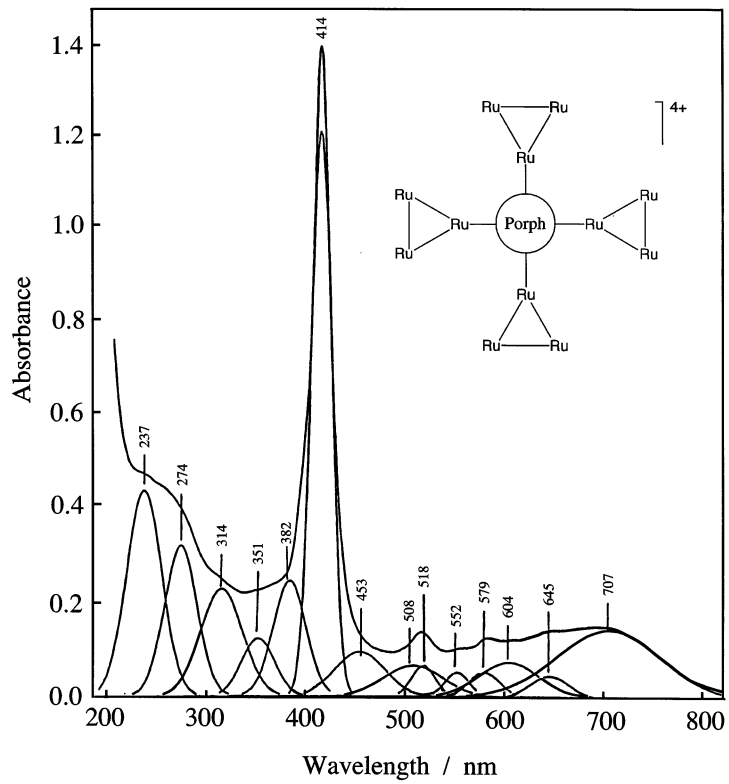

Fig. 17. Electronic spectrum of the tetracluster free-base porphyrin in acetonitrile solution (10^{-5} M) and the corresponding Gaussian components obtained by spectral deconvolution using the Grams/386 IBM/PC software.

intra-cluster bands in the 600–700 nm range, and the rise of a characteristic band at 920 nm. Similar changes have also been observed for the absorption bands at 314 and 351 nm which decay, whereas the absorption bands at 370 and 460 nm grow up, in agreement with their assignment as cluster-to-py charge-transfer transitions. At -1.0 V, there is a shift of the Soret band from 414 to 460 nm, whereas the cluster bands at 252 and 920 nm remain practically unchanged, supporting the reduction of the porphyrin center, yielding radical anion species [123,124]. At -1.6 V, the complex is reduced to the $Ru^{III,II,II}$ state, leading to a small bathochromic shift of the intracluster band at 920 nm, and to the rise of an absorption band at 520 nm, ascribed to the ruthenium-to-pyridine charge-transfer band. At this potential, a second reduction of the porphyrin ring takes place, leading to a pronounced decrease of the Soret band.

For the ZnTCP species, four successive redox waves assigned to $Ru_3^{IV,IV,III}O/Ru_3^{IV,III,III}O/Ru_3^{III,III,III}O/Ru_3^{III,III,II}O/Ru_3^{III,II,II}O$ processes were observed at 2.18,

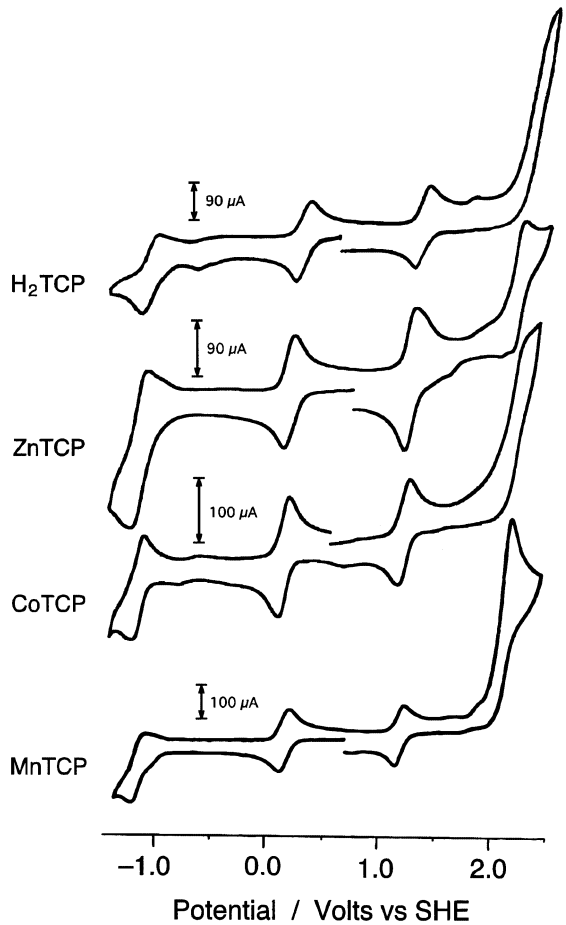

Fig. 18. Cyclic voltammograms of the tetracluster porphyrin complexes in acetonitrile, tetraethylammonium perchlorate 0.1 M, in the −1.5 to 2.5 V range.

1.19, 0.15 and −1.13 V, respectively, in acetonitrile solutions. The porphyrin electrochemical waves are superimposed on the cluster redox waves, but the corresponding redox processes can be identified by means of spectroelectrochemical measurements. At −1.0 V a composite reduction process takes place, involving the ZnTPyP/ZnTPyP$^-$ and $Ru_3^{III,III,II}O/Ru_3^{III,II,II}O$ redox couples, as deduced from the changes in the intracluster band at 920 nm, and in the Soret band at 467 nm, or from the rise of a zinc–porphyrin radical anion band around 700 nm. Further reduction in the −1.20 to −1.35 V range led to a decrease in the intensity of the Soret band, while the band around 700 nm disappeared, giving rise to a new band at 825 nm. This behavior was ascribed to the reduction of the porphyrin anion radical to the π-dianion [117,125]. Analogously, the redox wave in the 1.00–1.4 V range is significantly stronger and broader than that observed at 0.15 V, involving

more than one electrochemical process. The spectroelectrochemical measurements carried out at 1.25 V were consistent with the reversible oxidation/reduction of the cluster centers, ($Ru_3^{IV,III,III}O/Ru_3^{III,III,III}O$), while at 1.40 V there is a pronounced decay of the Soret and Q bands indicating the oxidation of the ZnTPyP center to its radical π-cation [117,126].

In the case of the CoTCP species, the cyclic voltammograms exhibit four reversible waves at 2.33, 1.25, 0.19 and −1.05 V, corresponding to the $Ru_3^{IV,IV,III}O/Ru_3^{IV,III,III}O/Ru_3^{III,III,III}O/Ru_3^{III,III,II}O/Ru_3^{III,II,II}O$ successive redox couples. Analogous to ZnTCP, the redox waves associated with the metalloporphyrin center are little evident in the cyclic voltammograms. Spectroelectrochemical measurements have demonstrated the composite nature of the reversible wave at 0.19 V, involving additionally the $Co^{III/II}$ process at $E° = 0.31$ V, responsible for significant changes in the Soret and Q bands. In the −0.5 to −0.8 V range, the Soret band is shifted from 412 to 421 nm while the intensity of the intracluster band at 913 nm is enhanced, indicating an appreciable electronic coupling between those subunits. Formation of porphyrin radical anion is usually indicated by the broadening and shift of the Soret band to about 450 nm, and by the appearance of absorption bands around 700 nm. Since these changes have not been observed, the electrochemical process around −0.6 V was ascribed to the $Co^{II/I}$ redox couple.

The cyclic voltammograms for the MnTCP complex exhibit the characteristic $Ru_3^{IV,IV,III}O/Ru_3^{IV,III,III}O/Ru_3^{III,III,III}O/Ru_3^{III,III,II}O/Ru_3^{III,II,II}O$ redox waves at ∼2, 1.17, 0.16 and −1.17 V respectively. Two additional processes are observed from the broadening and enhancement of the redox wave at 0.16 V, and by occurrence of a less-intense wave at −0.94 V. These two processes were characterized spectroelectrochemically as associated with the $Mn^{III/II}$ ($E° = 0.047$ V) and two successive porphyrin reductions, $Mn^{II}TPyP^0/Mn^{II}TPyP^-/Mn^{II}TPyP^{2-}$. It has been shown that the reduction of the porphyrin ring is accompanied by a shift and enhancement of the intracluster band at 913 nm, indicating appreciable electronic coupling between the cluster and the porphyrin moieties.

8.1. Tetraelectronic dioxygen reduction by CoTCP films

An interesting aspect is that CoTCP forms adherent and durable films onto glassy carbon surface, exhibiting a shiny violet color. Such films are insoluble in aqueous KNO_3 solutions, exhibiting a reversible redox wave at 0.22 V, as shown in Fig. 19. Its peak current is proportional to the scan rate, in agreement with the electrochemical behavior of redox-active immobilized species. The electronic spectrum of the CoTCP film is similar to those obtained in acetonitrile solutions, exhibiting the Soret and Q bands slightly shifted to 440, 555 and 610 nm, in addition to the intracluster band at 705 nm (Fig. 19). In comparison with the spectra of previously studied films of supramolecular porphyrin coordinated to four $[Ru(bipy)_2Cl]^+$ complex, [117,127] the CoTCP film spectrum is much less broadened. This comparison has been addressed, as evidence that the cobalt–porphyrin rings would be too far apart, for a strong interaction, due to the bulkiness of the peripheral ruthenium cluster groups.

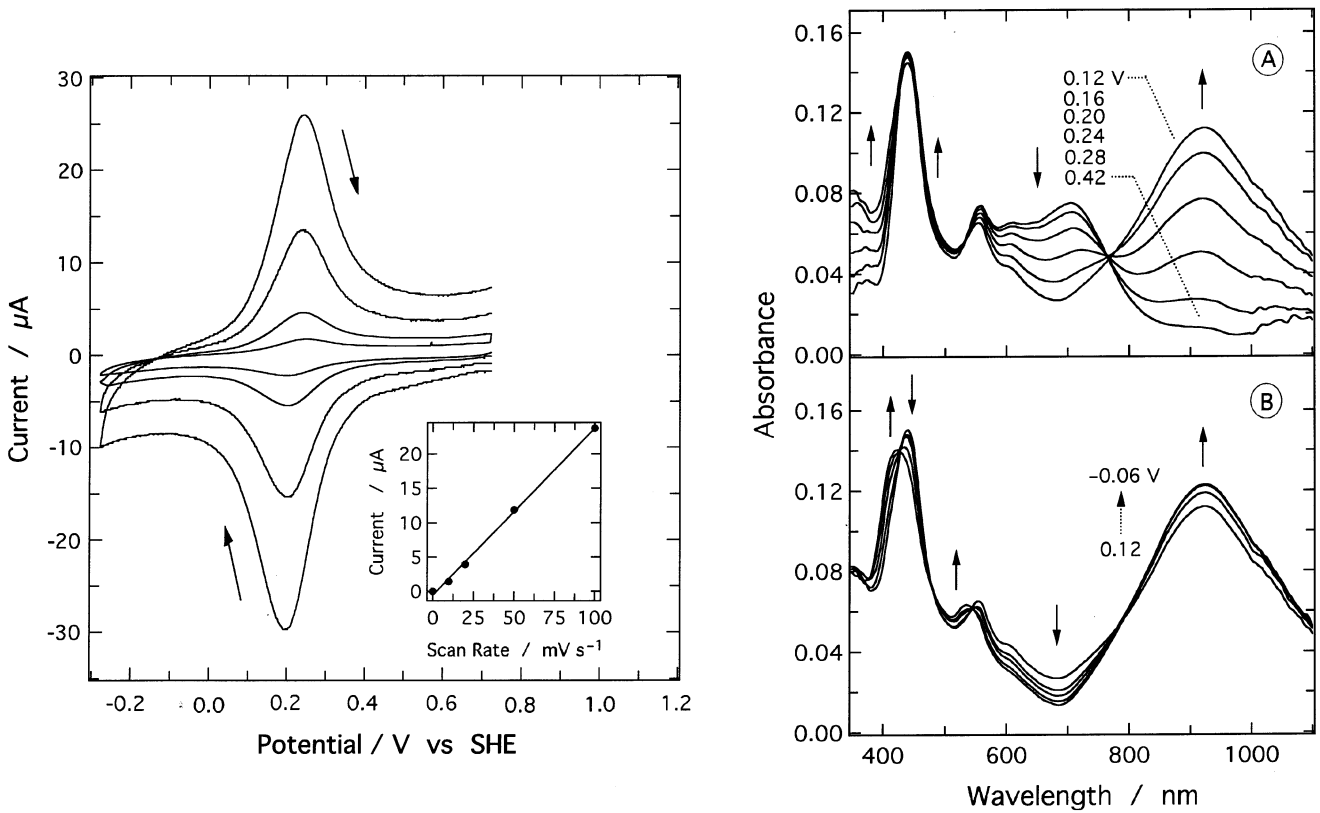

Fig. 19. Left: cyclic voltammograms of a CoTCP modified glassy carbon electrode (0.5 M KNO_3 aqueous solution). Inset: plot of the peak current intensities as a function of the scan rate. Right: spectroelectrochemical measurements of a film of CoTCP on a glassy carbon surface, in the (A) 0.12–0.42 V; and (B) −0.06 to 0.12 V.

The CoTCP-modified electrodes exhibit outstanding catalytic activity in the tetraelectronic reduction of dioxygen to water, giving rise to a sharp, intense cathodic peak around 0.2 V as illustrated in Fig. 20A. The current intensities follow a linear function of the square root of the scan rate, and the catalytic peak potential is close to the $E_{1/2}$ of the $Ru_3^{III,III,III}O/Ru_3^{III,III,II}O$ and $Co^{III/II}$ redox couples. The direct involvement of the ruthenium clusters on the catalytic activity has been ruled out from a comparison with the electrochemical behavior of the ZnTCP films. The electrochemical response of the ZnTCP modified electrodes, under similar conditions, exhibits no catalytic activity for the reduction of dioxygen. According to RDE and RRDE voltammetry (Figs. 20B and 21), the electrocatalytic reduction of dioxygen involves four electrons, yielding essentially water as the product. The kinetics involved as rather fast, and the reaction rate is not limited by mass transport or electron diffusion through the film. The enhanced activity has been attributed to the electronic activation of the cobalt–porphyrin center by the peripheral ruthenium cluster complexes, as supported from the spectroelectrochemical data indicating a significant electronic coupling within the supermolecule [133].

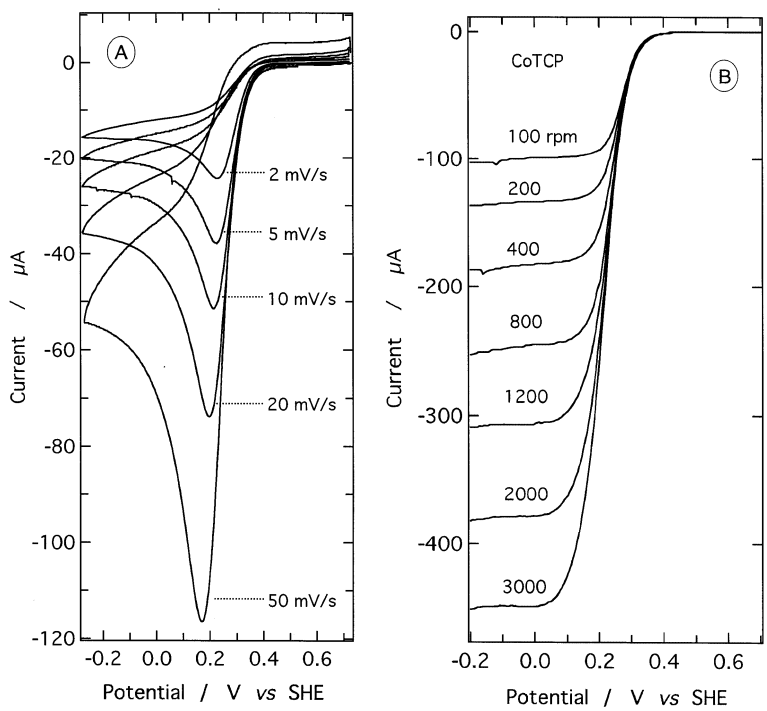

Fig. 20. (A) Cyclic voltammograms of an air-saturated solution at 2, 5, 10, 20 and 50 mV s^{-1}. (B) RDE voltammograms of a CoTCP modified rotating glassy carbon disk electrode in air-saturated aqueous solution. Electrolyte: 0.50 M KNO_3, acetate buffer 0.05 M, pH 4.7, $T = 25$°C.

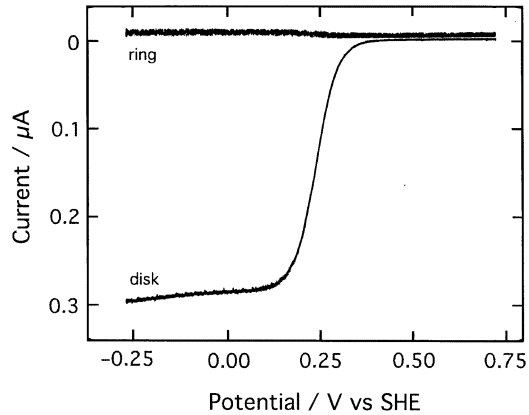

Fig. 21. Rotating ring disk electrode voltammogram of a CoTCP modified glassy carbon electrode (disk scan rate = 10 mV s^{-1}, $\omega = 1000$ rpm) in air-saturated 0.50 M KNO_3 aqueous solution, acetate buffer 0.05 M, pH 4.7, $T = 25$°C. The potential of the platinum ring electrode was set to 1.22 V in order to oxidize H_2O_2 to O_2.

8.2. Cytochrome P-450 catalytic activity of MnTCP

Manganese and iron–porphyrins provide interesting models of cytochrome P-450, since they can act as good oxygen atom transfer catalysts from iodosylarenes, tertiary amine oxides or hypochlorite to hydrocarbons, producing epoxides from alkenes and alcohols from alkanes. The active species consist of high-valence metal-oxo porphyrins, which are very reactive and sensitive to substituent effects at the *meso*-aryl and β-pyrrol carbon atoms. A remarkable catalytic activity has been reported for MnTCP [45], in the epoxidation of cyclooctene by iodosylbenzene, or in the hydroxylation of cyclohexane. Such experiments were carried out in a comparative way with the MnTPyP catalyst, in order to evaluate the role of the ruthenium clusters in the catalytic activity.

Both compounds catalyze efficiently and selectively the epoxidation of cyclooctene, with comparable yields (e.g. 80%, based on iodosylbenzene, reaction time = 1 h, catalyst concentration = 0.15 mM, catalyst/PhIO/cyclooctene molar ratio = 1:50:2000). However, when MnTCP was used as catalyst for the oxidation of a less-reactive substrate, such as cyclohexane, the results were significantly different. While the MnTPyP catalyst led to the formation of cyclohexanone (13%) and cyclohexanol (27%), MnTCP exclusively generated cyclohexanol (45%), keeping the same total yield (reaction time = 2 h, catalyst concentration 0.17 mM, catalyst/PhIO/cyclohexane molar ratio = 1:20:30 000).

In this type of system, high-valent metal-oxo porphyrins such as $O = Mn^{V}P$ have been proposed as the active species [128,129]. An oxidation process coupled with an oxygen atom transfer step is the most accepted mechanism to explain the high reactivity of the high-valent metal-oxo porphyrins. Such species are very reactive and usually cannot be detected under the experimental conditions employed for

catalysis. The spectroscopic changes recorded, using flow-cell techniques, for the MnTCP/iodoxylbenzene/cyclohexane system, are illustrated in Fig. 22. The recorded spectra are consistent with the rapid conversion of $Mn^{III}TCP$ to $O{=}Mn^{IV}TCP$, by comparison with the spectra of related oxomanganese(IV) species [130,131]. The observed changes in the absorption bands of the cluster, specially around 800 nm, are consistent with their partial oxidation to $Ru^{IV,III,III}$. Therefore, the formal redox potential for the $O{=}Mn^{IV}TCP/Mn^{III}TCP$ couple should be close to the $Ru_3^{IV,III,III}O/Ru_3^{III,III,III}O$ redox potential, i.e. 1.17 V. By this reasoning, the formal potential of the $O{=}Mn^{V}TCP/O{=}Mn^{IV}TCP$ redox pair should be higher than 1.17 V, and consequently, in the $O{=}Mn^{V}TCP$ species all peripheral clusters should be in the $Ru^{IV,III,III}$ state. As a consequence, the presence of the cluster groups in high oxidation states can enhance the activity of the $O{=}Mn^{V}$ center, by acting as electron withdrawing or electron receptor groups.

9. Final remarks

In addition to their intrinsic, relevant chemistry, the oxo-bridged trinuclear ruthenium clusters provide perhaps a unique way of generating chemical and supramolecular systems displaying truly remarkable reversible electron-transfer properties. Such electron-sponge like behavior is now starting to be exploited in biomimetic catalysis, resembling the iron–sulfur cofactors, as well as by enhancing the activity of the metalloporphyrins. Presumably, the strong electronic coupling observed for the ligand-bridged oligomeric species will support many relevant applications as molecular wires in electronic and molecular devices. Finally, the electrooptical properties arising from the combination of clusters and electrochemically active chromophores, at a wide range of oxidation states, will become

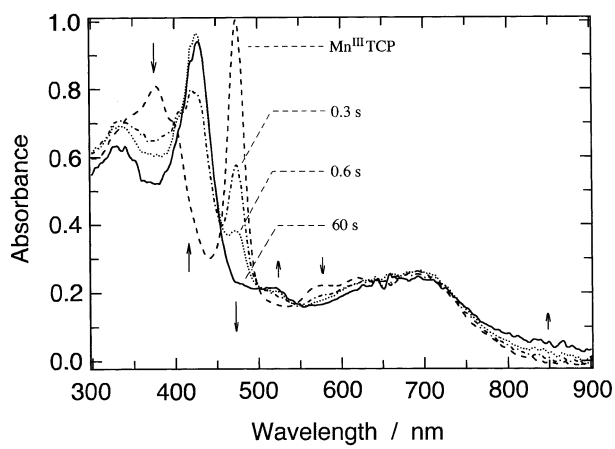

Fig. 22. Spectra of the solution obtained at different times by mixing equal volumes of $Mn^{III}TCP$ (0.02 mM) and iodosylbenzene (1.4 mM) in dichloroethane in a flow cell.

increasingly important for the design of outstanding electrochromic and non-linear optics devices.

Acknowledgements

The authors are very much indebted to FAPESP, CNPq and CAPES for the financial support.

References

[1] O. Almog, A. Bino, D. Garfinkel-Shweky, Inorg. Chim. Acta 213 (1993) 99.
[2] A. Spencer, G. Wilkinson, J. Chem. Soc. Dalton Trans. (1972) 1570.
[3] J.A. Baumann, D.J. Salmon, S.T. Wilson, T.J. Meyer, W.E. Hatfield, Inorg. Chem. 17 (1978) 3342.
[4] H.E. Toma, C.J. Cunha, C. Cipriano, Inorg. Chim. Acta 154 (1988) 63.
[5] A.N. Zhilyaev, T.A. Fomina, S.B. Katser, I.B. Baranovskii, Russ. J. Inorg. Chem. 39 (1994) 856.
[6] S. Davis, R.S. Drago, Inorg. Chem. 27 (1988) 4759.
[7] M. Abe, Y. Sasaki, T. Yamaguchi, T. Ito, Bull. Chem. Soc. Jpn 65 (1992) 1585.
[8] A. Ohto, A. Tokiwa-Yamamoto, M. Abe, T. Ito, Y. Sasaki, K. Umakoshi, R.D. Cannon, Chem. Lett. (1995) 97.
[9] C. Oldham, Prog. Inorg. Chem. 10 (1968) 223.
[10] A. Dobson, S.D. Robinson, Platinum Metals Rev. 1976 (1976) 56.
[11] J. Catterick, P. Thornton, Adv. Inorg. Chem. Radiochem. 20 (1977) 291.
[12] R.D. Cannon, R.P. White, Prog. Inorg. Chem. 36 (1988) 195.
[13] B.O. West, Polyhedron 8 (1989) 219.
[14] T.M. Buslaeva, S.N. Red'kina, O.V. Rudnitskaya, Russ. J. Coord. Chem. 25 (1999) 1.
[15] Y. Sasaki, A. Tokiwa, T. Ito, J. Am. Chem. Soc. 109 (1987) 6341.
[16] M.K. Johnson, D.B. Powell, R.D. Cannon, Spectrochim. Acta A 37 (1981) 995.
[17] M. Abe, Y. Sasaki, Y. Yamada, K. Tsukahara, S. Yano, T. Ito, Inorg. Chem. 34 (1995) 4490.
[18] Y. Sasaki, Y. Yoshida, A. Ohto, A. Tokiwa, T. Ito, H. Kobayashi, N. Uryu, I. Mogi, Chem. Lett. (1993) 69.
[19] Y. Sasaki, M. Suzuki, A. Nagasawa, A. Tokiwa, M. Ebihara, T. Yamaguchi, C. Kabuto, T. Ochi, T. Ito, Inorg. Chem. 30 (1991) 4903.
[20] A. Spencer, G. Wilkinson, J. Chem. Soc. Dalton Trans. (1974) 786.
[21] H.E. Toma, C. Cipriano, Monatsh. Chem. 120 (1989) 815.
[22] H.E. Toma, C.J. Cunha, Can. J. Chem. 67 (1989) 1632.
[23] S. Cosnier, A. Deronzier, A. Llobet, J. Electroanal. Chem. 280 (1990) 213.
[24] H.E. Toma, M.A.L. Olive, Polyhedron 13 (1994) 2647.
[25] A.D.P. Alexiou, H.E. Toma, J. Chem. Res. (S) (1993) 464.
[26] J.A. Baumann, S.T. Wilson, D.J. Salmon, P.L. Hood, T.J. Meyer, J. Am. Chem. Soc. 101 (1979) 2916.
[27] K. Nagase, H. Yokobayashi, A. Watanabe, H. Ishikawa, T. Matsumoto, H. Kido, T. Ito, Netsu Sokutei 20 (1993) 66.
[28] M. Abe, Y. Sasaki, Y. Yamada, K. Tsukahara, S. Yano, T. Yamaguchi, M. Tominaga, I. Taniguchi, T. Ito, Inorg. Chem. 35 (1996) 6724.
[29] J. Araujo Jr., S. Nikolaou, A.D.P. Alexiou, H.E. Toma, Monatsh. Chem. 128 (1997) 759.
[30] A.D.P. Alexiou, H.E. Toma, J. Chem. Res. (S) (1997) 338.
[31] H.E. Toma, A.D.P. Alexiou, Electrochim. Acta 38 (1993) 975.
[32] H. Kido, H. Nagino, T. Ito, Chem. Lett. (1996) 745.

[33] T. Ito, T. Hamaguchi, H. Nagino, T. Yamaguchi, J. Washington, C.P. Kubiak, Science 277 (1997) 660.
[34] F.A. Cotton, J.G. Norman Jr., Inorg. Chim. Acta 6 (1972) 411.
[35] K. Ota, H. Sasaki, T. Matsui, T. Hamaguchi, T. Yamaguchi, T. Ito, H. Kido, C.P. Kubiak, Inorg. Chem. 38 (1999) 4070.
[36] T. Yamaguchi, N. Imai, T. Ito, C.P. Kubiak, Bull. Chem. Soc. Jpn 73 (2000) 1205.
[37] T.Y. Dong, H.S. Lee, T.Y. Lee, C.F. Hsieh, J. Chin. Chem. Soc. 39 (1992) 393.
[38] H.E. Toma, A.D.P. Alexiou, J. Chem. Res. (S) (1995) 134.
[39] H.E. Toma, A.D.P. Alexiou, J. Braz. Chem. Soc. 6 (1995) 267.
[40] M. Abe, Y. Sasaki, A. Nagasawa, T. Ito, Bull. Chem. Soc. Jpn 65 (1992) 1411.
[41] C. Bilgrien, S. Davis, R.S. Drago, J. Am. Chem. Soc. 109 (1987) 3786.
[42] H.E. Toma, S. Nikolaou, J. Chem. Res. (S) (2000) 326.
[43] S. Nikolaou, H.E. Toma, Polyhedron 20 (2001) 253.
[44] M. Abe, A. Sato, T. Inomata, T. Kondo, K. Uosaki, Y. Sasaki, J. Chem. Soc. Dalton Trans. (2000) 2693.
[45] S. Dovidauskas, H.E. Toma, K. Araki, H. Sacco, Y. Iamamoto, Inorg. Chim. Acta 305 (2000) 206.
[46] I.S. Zavarine, C.P. Kubiak, T. Yamaguchi, K. Ota, T. Matsui, T. Ito, Inorg. Chem. 39 (2000) 2696.
[47] M. Abe, M. Tanaka, K. Umakoshi, Y. Sasaki, Inorg. Chem. 38 (1999) 4146.
[48] T. Ito, T. Hamaguchi, H. Nagino, T. Yamaguchi, H. Kido, I.S. Zavarine, T. Richmond, J. Washington, C.P. Kubiak, J. Am. Chem. Soc. 121 (1999) 4625.
[49] S.A. Simanova, A.N. Belyaev, V.I. Bashmakov, O.N. Troshina, A.V. Shchukarev, F.I. Danilova, Russ. J. General Chem. 63 (1993) 1378.
[50] H.E. Toma, A.D. P. Alexiou, S. Nikolaou, S. Dovidauskas, Magn. Reson. Chem. 37 (1999) 322.
[51] S. Davis, R.S. Drago, J. Chem. Soc. Chem. Commun. (1990) 250.
[52] M.K. Johnson, R.D. Cannon, D.B. Powell, Spectrochim. Acta 38A (1982) 307.
[53] M. Velayutham, C.S. Gopinath, S. Subramanian, Chem. Phys. Lett. 249 (1996) 71.
[54] S. Ye, H. Akutagawa, K. Uosaki, Y. Sasaki, Inorg. Chem. 34 (1995) 4527.
[55] S.T. Wilson, R.F. Bondurant, T.J. Meyer, D.J. Salmon, J. Am. Chem. Soc. 97 (1975) 2285.
[56] C.J. Jia, F.Y. Jin, M.Y. Huang, Y.Y. Jiang, Reactive Polym. 23 (1994) 33.
[57] F.A. Cotton, J.G. Norman, A. Spencer, G. Wilkinson, Chem. Commun. (1971) 967.
[58] M. Mukaida, M. Kusakari, T. Togano, T. Isomae, T. Nomura, T. Ishimori, Bull. Chem. Soc. Jpn 48 (1975) 1095.
[59] E.A. Berngardt, I.N. Marov, V.K. Belyaeva, Russ. J. Inorg. Chem. 40 (1995) 1455.
[60] H. Kobayashi, N. Uryû, I. Mogi, R. Miyamoto, Y. Ohba, M. Iwaizumi, Y. Sasaki, A. Ohto, T. Ito, Bull. Chem. Soc. Jpn 68 (1995) 2551.
[61] A. Ohto, Y. Sasaki, T. Ito, Inorg. Chem. 33 (1994) 1245.
[62] H. Kobayashi, N. Uryû, I. Mogi, R. Miyamoto, Y. Ohba, M. Iwaizumi, Y. Sasaki, A. Ohto, M. Suwabe, T. Ito, Bull. Chem. Soc. Jpn 69 (1996) 3163.
[63] H. Kobayashi, N. Uryû, A. Tokiwa, T. Yamaguchi, Y. Sasaki, T. Ito, Bull. Chem. Soc. Jpn 65 (1992) 198.
[64] Y. Sasaki, A. Nagasawa, A. Tokiwa-Yamamoto, T. Ito, Inorg. Chim. Acta 212 (1993) 175.
[65] Y. Sasaki, K. Umakoshi, T. Imamura, A. Kikuchi, A. Kishimoto, Pure Appl. Chem. 69 (1997) 205.
[66] G. Powell, D.T. Richens, A.K. Powell, Inorg. Chim. Acta 213 (1993) 147.
[67] H.E. Toma, C. Cipriano, J. Electroanal. Chem. 263 (1989) 313.
[68] A.B.P. Lever, Inorg. Chem. 29 (1990) 1271.
[69] J.E. Huheey, J. Phys. Chem. 69 (1965) 3284.
[70] R.S. Nicholson, I. Shain, Anal. Chem. 36 (1964) 706.
[71] D. Akashi, H. Kido, Y. Sasaki, T. Ito, Chem. Lett. (1992) 143.
[72] H.E. Toma, F.M. Matsumoto, C. Cipriano, J. Electroanal. Chem. 346 (1993) 261.
[73] P. Legzdins, R.W. Mitchell, G.L. Rempel, J.D. Ruddick, G. Wilkinson, J. Chem. Soc. (A) (1970) 3322.

[74] R.W. Mitchell, A. Spencer, G. Wilkinson, J. Chem. Soc. Dalton Trans. (1973) 846.
[75] S.A. Fouda, B.C.Y. Hui, G.L. Rempel, Inorg. Chem. 17 (1978) 3213.
[76] C.P. Nicolaides, N.J. Coville, J. Mol. Catal. 24 (1984) 375.
[77] Y. Sasson, G.L. Rempel, Can. J. Chem. 52 (1974) 3825.
[78] Y. Sasson, G.L. Rempel, Tetrahedron Lett. 47 (1974) 4133.
[79] D.J. Milner, R. Whelan, J. Organomet. Chem. 152 (1978) 193.
[80] J. Thivolle-Cazat, I. Tkatchenko, J. Chem. Soc. Chem. Commun. (1982) 1128.
[81] T. Szymanska-Buzar, J.J. Ziólkowski, J. Mol. Catal. 11 (1981) 371.
[82] A.M. Trzeciak, T. Szymanska-Buzar, J.J. Ziólkowski, J. Mol. Catal. 10 (1981) 69.
[83] S. Ito, K. Aihara, M. Matsumoto, Tetrahedron Lett. 24 (1983) 5249.
[84] G. Powell, D.T. Richens, L. Khan, J. Chem. Res. (S) (1994) 506.
[85] D.E. Bergbreiter, D.R. Treadwell, Reactive Polym. 12 (1990) 291.
[86] J.A. Baumann, D.J. Salmon, S.T. Wilson, T.J. Meyer, Inorg. Chem. 18 (1979) 2472.
[87] M.B. Robin, P. Day, Adv. Inorg. Chem. Radiochem. 10 (1967) 247.
[88] H.E. Toma, P.S. Santos, C. Cipriano, Spectrosc. Lett. 21 (1988) 909.
[89] H.E. Toma, A.B.P. Lever, Inorg. Chem. 25 (1986) 176.
[90] H.E. Toma, P.R. Auburn, E.S. Dodsworth, M.N. Golovin, A.B.P. Lever, Inorg. Chem. 26 (1987) 4257.
[91] H.E. Toma, P.S. Santos, A.B.P. Lever, Inorg. Chem. 27 (1988) 3850.
[92] P. Ford, D.P.F. Rudd, R. Gaunder, H. Taube, J. Am. Chem. Soc. 90 (1968) 1187.
[93] H.E. Toma, C. Creutz, Inorg. Chem. 16 (1977) 545.
[94] J.B. Flanagan, S. Margel, A.J. Bard, F.C. Anson, J. Am. Chem. Soc. 100 (1978) 4248.
[95] K. Itaya, T. Ataka, S. Toshima, J. Am. Chem. Soc. 104 (1982) 4767.
[96] A.B. Bocarsly, S.J. Sinha, J. Electroanal. Chem. 140 (1982) 167.
[97] V.D. Neff, K. Itaya, I. Uchida, Acc. Chem. Res. 19 (1986) 162.
[98] L.F. Schneemeyer, S.E. Spengler, D.W. Murphy, Inorg. Chem. 24 (1985) 3044.
[99] C.A. Lundgreen, R.W. Murray, Inorg. Chem. 27 (1988) 933.
[100] H.E. Toma, R.M. Serrasqueiro, R.C. Rocha, G.J.F. Demets, H. Winnischofer, K. Araki, P.E.A. Ribeiro, C.L. Donnici, J. Photochem. Photobiol. 135 (2000) 185.
[101] M.K. Wall, S. Akimoto, T. Yamazaki, N. Ohta, I. Yamazaki, T. Sakuma, H. Kido, Bull. Chem. Soc. Jpn 72 (1999) 1475.
[102] L. Angnes, C.M.N. Azevedo, K. Araki, H.E. Toma, Anal. Chim. Acta 329 (1996) 91.
[103] K. Araki, L. Angnes, C.M.N. Azevedo, H.E. Toma, J. Electroanal. Chem. 397 (1995) 205.
[104] F. Bedioui, J. Devynck, C. Bied-Charreton, Acc. Chem. Res. 28 (1995) 30.
[105] M.A. Gilles-Gonzalez, G. Gonzales, M.F. Perutz, L. Kiger, M.C. Marden, C. Poyart, Biochemistry 33 (1994) 8067.
[106] K. Jayaraj, J. Terner, A. Gold, D.A. Roberts, R.N. Austin, D. Mandon, R. Weiss, E. Bill, M. Müther, A.X. Trautwein, Inorg. Chem. 35 (1996) 1632.
[107] C. Shi, F.C. Anson, Inorg. Chim. Acta 225 (1994) 215.
[108] J.R.L. Smith, Metalloporphyrins in Catalytic Oxidations, Marcel Dekker, New York, 1994.
[109] B. Steiger, F.C. Anson, Inorg. Chem. 33 (1994) 5767.
[110] J. Onuki, A.V. Ribas, M.H. G. Medeiros, K. Araki, H.E. Toma, L.H. Catalani, P. DiMascio, Photochem. Photobiol. 63 (1996) 272.
[111] H.E. Toma, K. Araki, J. Chem. Res. (S) (1990) 82.
[112] H.E. Toma, K. Araki, Inorg. Chim. Acta. 179 (1991) 293.
[113] H.E. Toma, K. Araki, Coord. Chem. Rev. 196 (2000) 307.
[114] V. Krishnan, E.E. Batova, V.Y. Shafirovich, J. Photochem. Photobiol. 84 (1994) 233.
[115] M.R. Wasielewski, Chem. Rev. 92 (1992) 435.
[116] R. Bonnett, Chem. Soc. Rev. (1995) 19.
[117] K. Araki, H.E. Toma, J. Photochem. Photobiol. 83 (1994) 245.
[118] J. Bernard, M. Orrit, R.I. Personov, A.D. Samoilenko, Chem. Phys. Lett. 164 (1989) 377.
[119] M.J. Gunter, M.R. Johnston, J. Chem. Soc. Chem. Commun. (1992) 1163.
[120] T.J. Schaafsma, Sol. Energy Mater. Sol. Cells 38 (1995) 349.
[121] H.E. Toma, K. Araki, E.O. Silva, Monatsh. Chem. 129 (1998) 975.

[122] S. Dovidauskas, K. Araki, H.E. Toma, J. Porph. Phthalocyanines 4 (2000) 727.
[123] K. Araki, H.E. Toma, J. Chem. Res. (M) (1994) 1501.
[124] K. Araki, H.E. Toma, J. Coord. Chem. 30 (1993) 9.
[125] E.V. Caemelbecke, W. Kutner, K.M. Kadish, Inorg. Chem. 32 (1993) 438.
[126] X.H. Mu, F.A. Schultz, Inorg. Chem. 31 (1992) 3351.
[127] K. Araki, L. Angnes, H.E. Toma, Adv. Mater. 7 (1995) 554.
[128] M.J. Gunter, P. Turner, Coord. Chem. Rev. 108 (1991) 115.
[129] B. Meunier, Chem. Rev. 92 (1992) 1411.
[130] J.A. Smegal, C.L. Hill, J. Am. Chem. Soc. 105 (1983) 3515.
[131] R.S. Czernuszewicz, Y.O. Su, M.K. Stern, K.A. Macor, D. Kim, J.T. Groves, T.G. Spiro, J. Am. Chem. Soc. 110 (1988) 4158.
[132] G. Powell, D.T. Richens, A. Bino, Inorg. Chim. Acta 232 (1995) 167.
[133] K. Araki, S. Dovidauskas, H. Winnischofer, A.D.P. Alexiou, H.E. Toma, J. Electroanal. Chem. 498 (2001) 152.